

# The dynamic stiffness matrix based on the extended separation-of-variables type solution for the free vibration of orthotropic rectangular thin plates

Shiyi Mei<sup>a</sup>, Colin Caprani<sup>a,\*</sup>, Daniel Cantero<sup>b</sup>

<sup>a</sup>*Department of Civil Engineering, Monash University, Melbourne, Victoria, Australia*

<sup>b</sup>*Department of Structural Engineering, Norwegian University of Science & Technology  
NTNU, Trondheim, Norway*

---

## Abstract

The dynamic stiffness matrix (DSM) based on the extended separation-of-variables (SOV) type mode solution is developed for the free vibration analysis of an orthotropic rectangular thin plate with general homogeneous boundary conditions. The method combines the advantages of the DSM method and the SOV method. The SOV type solution satisfies the governing differential equation derived from Rayleigh's principle and is used to formulate the dynamic stiffness matrices. Owing to the characteristics of the SOV type solution, the fully clamped boundary condition problem associated with the Wittrick–Williams algorithm is resolved. The enhanced algorithm is further proposed to solve dynamic stiffness matrices, rather than solving eigenvalue equations. A numerical technique for mode shape computation is also introduced. The accuracy of the proposed method is validated through numerical experiments.

---

## 1. Introduction

Rectangular plates play an important role in various engineering fields, including civil, mechanical, and aerospace engineering [3]. The free vibration of plates has been a fundamental research problem for over two centuries.

---

\*Corresponding author

Email addresses: `shiyi.mei1@monash.edu` (Shiyi Mei), `colin.caprani@monash.edu` (Colin Caprani), `daniel.cantero@ntnu.no` (Daniel Cantero)

5 The earliest exact solutions for this problem are the Navier [21] and Levy  
6 [14] solutions, which require at least one pair of opposite edges to be simply  
7 supported or guided. To solve problems with other boundary conditions, ap-  
8 proximate solutions such as the Rayleigh–Ritz method [13] and the Galerkin  
9 method [12] have been widely applied. For these approximation methods,  
10 beam functions, polynomials, trigonometric functions, and their combina-  
11 tions [16] are commonly used as the assumed approximate functions. The  
12 accuracy of these solutions depends on how well the assumed approximate  
13 functions represent the displacement of the plate.

14 Besides the approximation methods, several analytical methods have been  
15 developed over the past decades, including the Kantorovich-Krylov method  
16 [9, 10], the symplectic eigenfunction expansion method [32, 25], the separation-  
17 of-variable (SOV) method [29], the dynamic stiffness matrix (DSM) method  
18 [2], and series expansion-based methods [24]. The series expansion-based  
19 methods include the superposition method [22, 7], Fourier series method  
20 [11, 17], the finite integral transform method [15, 33], and other series meth-  
21 ods. These methods represent the plate displacement in terms of an infinite  
22 series and mostly are capable of handling any general boundary conditions.  
23 However, sufficient truncation of the series is required to ensure the accuracy  
24 and convergence of the results, and the eigenvalue equation is generally dif-  
25 ficult to express explicitly. Therefore, solving the corresponding eigenvalue  
26 problem can be computationally expensive.

27 Despite being a powerful method for the dynamic analysis of plate as-  
28 semblies, the finite element method (FEM) requires a sufficient number of  
29 elements and is computationally expensive to accurately capture higher-order  
30 modes. Thus, the DSM method was developed as an accurate and efficient  
31 analytical approach to alternatively solve complex plate structures [4, 5]. The  
32 DSM can be considered as an analytical FEM since the mode functions of  
33 the plate are expressed by analytical solutions, where Levy-type solution [6]  
34 or components of infinite Fourier series [1, 19] are applied. To avoid solving  
35 the cumbersome transcendental frequency equation directly, the Wittrick-  
36 Williams (W-W) algorithm [23] is applied to the eigenvalue problem. The  
37 W-W algorithm determines the lower and upper bounds of natural frequen-  
38 cies rather than solving the frequency equation directly. Thus, the DSM has  
39 the potential to be effectively and systematically solved using the W-W algo-  
40 rithm. However, a critical part in applying the W-W algorithm is to priorly  
41 determine all natural frequencies of the fully clamped structure within the  
42 interested frequency range. Strategies such as using a sufficiently fine mesh

43 or including a sufficient number of terms in series expansions [1] can ensure  
 44 that all fully clamped frequencies are accounted for, thereby maintaining the  
 45 accuracy of the algorithm. However, these approaches are computationally  
 46 expensive and complex, posing a significant obstacle to the wider adoption  
 47 and application of the DSM method based on the W-W algorithm [8]. To  
 48 resolve the fully clamped plate problem, Liu and Banerjee [18] suggested  
 49 that the frequencies can be indirectly obtained from the simply supported  
 50 plate problem, where the Navier solution serves as the analytical solution.  
 51 This provides a significant enhancement to the W-W algorithm, increasing  
 52 the efficiency of applying DSM methods. However, the solutions are not ex-  
 53 plicit and closed-form, but are expressed in an infinite series form, where a  
 54 sufficient number of truncation terms is required to ensure accuracy.

55 Inspired by the Navier and Levy solutions, Xing and Liu [29] proposed  
 56 the SOV method, which provides concise and explicit eigensolutions. The  
 57 mode shape function has a separable form,  $\phi(x)\psi(y)$ , requiring only one  $\phi(x)$   
 58 and one  $\psi(y)$  for each mode order, allowing each eigenvalue equation to be  
 59 explicitly expressed. However, this SOV method is not suitable to deal with  
 60 plates with free boundary conditions. Therefore, an extended SOV method  
 61 [26, 27] based on the Rayleigh quotient was proposed to accommodate plates  
 62 with all four classical boundary conditions, i.e., simply supported, clamped,  
 63 guided, and free. Based on the Rayleigh quotient model, alternative iterative  
 64 and improved SOV methods have been subsequently proposed [28]. Although  
 65 SOV methods provide concise closed-form analytical solutions, they require  
 66 solving a specific set of highly nonlinear eigenvalue equations for each type  
 67 of boundary condition. However, even when considering only the four classic  
 68 homogeneous cases, it becomes evident that 55 different boundary condition  
 69 combinations exist for a rectangular plate, making the process tedious.

70 In this study, the SOV method is extended to analyze the vibrations of  
 71 plates with elastically restrained edges. The extended SOV type solution is  
 72 then employed to construct the dynamic stiffness matrices, which accommo-  
 73 date all general homogeneous boundary conditions. By taking advantage of  
 74 both the SOV and DSM methods, an enhanced W-W algorithm is developed  
 75 to solve the eigenvalue problem without directly solving the eigenvalue equa-  
 76 tions. This enhanced approach resolves the challenge of determining fully  
 77 clamped frequencies, a well-known limitation in the application of the W-W  
 78 algorithm. In addition, a novel numerical technique has been proposed to  
 79 compute the mode shape coefficients.

## 80 2. Mathematical model

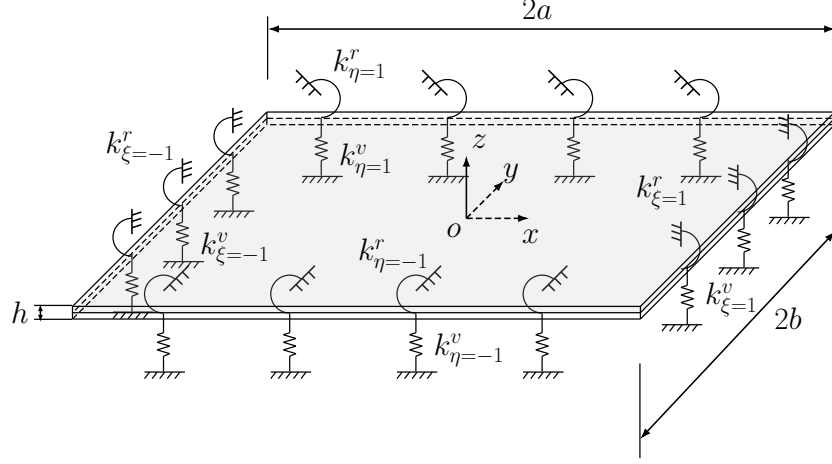


Figure 1: The orthotropic rectangular plate with all edges elastically restrained.

81 Consider a thin orthotropic rectangular plate of length  $2a$  and width  
 82  $2b$ , with all four edges restrained by vertical translational springs  $k^v$  and  
 83 rotational springs  $k^r$ , as shown in Figure 1. The coordinate origin is located  
 84 at the center of the plate.

85 The governing differential equation for the free vibration of a thin or-  
 86 thotropic plate is given by [28]:

$$D_{11} \frac{\partial^4 w}{\partial \xi^4} + 2D_3 \alpha^2 \frac{\partial^4 w}{\partial \xi^2 \partial \eta^2} + D_{22} \alpha^4 \frac{\partial^4 w}{\partial \eta^4} = \rho h \alpha^4 \omega^2 w, \quad (1)$$

87 where  $\alpha = a/b$  is the aspect ratio;  $\xi = x/a$  and  $\eta = y/b$  are the normalized  
 88 coordinates, and the bending stiffness parameters are defined as:

$$\begin{aligned} D_{11} &= \frac{E_1 h^3}{12(1 - v_{12}v_{21})}, & D_{22} &= \frac{E_2 h^3}{12(1 - v_{12}v_{21})}, \\ D_{66} &= \frac{G_{12} h^3}{12}, & D_{12} &= v_{12}D_{22} = v_{21}D_{11}, & D_3 &= D_{12} + 2D_{66}, \end{aligned} \quad (2)$$

89 where  $\rho$  and  $h$  denote the mass density and thickness of the plate, respec-  
 90 tively;  $E_1$  and  $E_2$  are the Young's moduli in the  $x$ - and  $y$ -directions, respec-  
 91 tively;  $G_{12}$  is the shear modulus, and  $v_{12}$  and  $v_{21}$  are the Poisson's ratios.

92 Instead of solving the free vibration of the thin orthotropic plate using  
 93 Equation (1), it is suggested that the vibration of the thin plate can also be  
 94 solved using the Rayleigh quotient variational principle [26]:

$$\delta U_{mag} = \omega^2 \delta T_0, \quad (3)$$

95 where  $\delta$  denotes variation,  $U_{mag}$  is the magnitude of the potential energy of  
 96 the plate, and  $\omega^2 T_0$  represents the magnitude of the kinetic energy of the  
 97 plate. The potential energy of the plate can be expressed as [27]:

$$U^I = \frac{1}{2} \iint \left[ D_{11} \left( \frac{\partial^2 W}{\partial x^2} \right)^2 + 2D_{12} \frac{\partial^2 W}{\partial x^2} \frac{\partial^2 W}{\partial y^2} + D_{22} \left( \frac{\partial^2 W}{\partial y^2} \right)^2 \right. \\ \left. + 4D_{66} \left( \frac{\partial^2 W}{\partial x \partial y} \right)^2 \right] dx dy. \quad (4)$$

98 And the kinetic energy is:

$$T = \frac{1}{2} \iint \rho h \left( \frac{\partial W}{\partial t} \right)^2 dx dy. \quad (5)$$

99 Assuming the solution of the deflection  $W(x, y; t) = w(x, y)e^{i\omega t}$  for har-  
 100 monic plate motion, where  $i = \sqrt{-1}$ ,  $w(x, y)$  is the mode shape, and  $\omega$  is the  
 101 radial frequency. By substituting  $W(x, y; t) = w(x, y)e^{i\omega t}$  into Equations (4)  
 102 and (5) and expressing the system in dimensionless coordinates, we have:

$$U_{mag}^I = \frac{ab}{2} \iint \left[ \frac{D_{11}}{a^4} \left( \frac{\partial^2 w}{\partial \xi^2} \right)^2 + \frac{2D_{12}}{a^2 b^2} \frac{\partial^2 w}{\partial \xi^2} \frac{\partial^2 w}{\partial \eta^2} + \frac{D_{22}}{b^4} \left( \frac{\partial^2 w}{\partial \eta^2} \right)^2 \right. \\ \left. + \frac{4D_{66}}{a^2 b^2} \left( \frac{\partial^2 w}{\partial \xi \partial \eta} \right)^2 \right] d\xi d\eta, \quad (6)$$

103 and

$$T = \omega^2 \frac{ab}{2} \rho h \iint w^2 d\xi d\eta = \omega^2 T_0, \quad (7)$$

104 The separable form of the mode shape function  $w(\xi, \eta)$  is given by:

$$w(\xi, \eta) = \phi(\xi)\psi(\eta), \quad (8)$$

105 where  $\phi(\xi)$  and  $\psi(\eta)$  can be expressed as:

$$\phi(\xi) = A_1 \sin(\alpha_1 \xi) + A_2 \cos(\alpha_1 \xi) + A_3 \sinh(\beta_1 \xi) + A_4 \cosh(\beta_1 \xi), \quad (9a)$$

$$\psi(\eta) = B_1 \sin(\alpha_2 \eta) + B_2 \cos(\alpha_2 \eta) + B_3 \sinh(\beta_2 \eta) + B_4 \cosh(\beta_2 \eta). \quad (9b)$$

106 Based on Equation (3), the frequencies  $\omega_x$  and  $\omega_y$ , corresponding to the  
 107 mode shapes  $\phi(\xi)$  and  $\psi(\eta)$ , respectively, are assumed to be independent of  
 108 each other.

### 109 2.1. Dynamic stiffness matrix corresponding to $\omega_x$

110 For given general homogeneous boundary conditions, we can first assume  
 111 that the mode shape  $\psi(\eta)$  corresponding to the  $y$ -direction is known. Sup-  
 112 posing the edges of the plate in both the  $x$ - and  $y$ -directions are elastically  
 113 restrained by homogeneous vertical translational and rotational springs. The  
 114 vertical translational and rotational springs at the  $\xi = -1$  end are defined  
 115 as  $k_{\xi=-1}^v$  and  $k_{\xi=-1}^r$ , respectively, and at the  $\xi = 1$  end as  $k_{\xi=1}^v$  and  $k_{\xi=1}^r$ ,  
 116 respectively. Thus, the potential energy along the supported edge in the  
 117  $x$ -direction can be expressed by:

$$\begin{aligned} U^{II} = & \int \left[ k_{\xi=-1}^r \left( \frac{\partial W}{\partial x} \right)^2 + k_{\xi=-1}^v (W)^2 \right]_{x=-a} dy \\ & + \int \left[ k_{\xi=1}^r \left( \frac{\partial W}{\partial x} \right)^2 + k_{\xi=1}^v (W)^2 \right]_{x=a} dy. \end{aligned} \quad (10)$$

118 From Equation (10), the magnitude of total potential energy along the edges  
 119 in the  $x$ -direction is obtained as:

$$\begin{aligned} U_{mag}^{II} = & ab \int \left[ \frac{k_{\xi=-1}^r}{a^3} \left( \frac{\partial w}{\partial \xi} \right)^2 + \frac{k_{\xi=-1}^v}{a} (w)^2 \right]_{\xi=-1} d\eta \\ & + ab \int \left[ \frac{k_{\xi=1}^r}{a^3} \left( \frac{\partial w}{\partial \xi} \right)^2 + \frac{k_{\xi=1}^v}{a} (w)^2 \right]_{\xi=1} d\eta. \end{aligned} \quad (11)$$

120 The magnitude of potential energy of the plate in the  $x$ -direction can be  
 121 obtained from Equations (6) and (11) as:

$$\begin{aligned}
 U_{mag} &= U_{mag}^I + U_{mag}^{II} \\
 &= \frac{ab}{2} \iint \left[ \frac{D_{11}}{a^4} \left( \frac{\partial^2 w}{\partial \xi^2} \right)^2 + \frac{2D_{12}}{a^2 b^2} \frac{\partial^2 w}{\partial \xi^2} \frac{\partial^2 w}{\partial \eta^2} + \frac{D_{22}}{b^4} \left( \frac{\partial^2 w}{\partial \eta^2} \right)^2 \right. \\
 &\quad \left. + \frac{4D_{66}}{a^2 b^2} \left( \frac{\partial^2 w}{\partial \xi \partial \eta} \right)^2 \right] d\xi d\eta + ab \int \left[ \frac{k_{\xi=1}^r}{a^3} \left( \frac{\partial w}{\partial \xi} \right)^2 + \frac{k_{\xi=1}^v}{a} (w)^2 \right]_{\xi=1} d\eta \\
 &\quad + ab \int \left[ \frac{k_{\xi=-1}^r}{a^3} \left( \frac{\partial w}{\partial \xi} \right)^2 + \frac{k_{\xi=-1}^v}{a} (w)^2 \right]_{\xi=-1} d\eta
 \end{aligned}
 \tag{12}$$

122 By substituting Equation (8) into Equation (12), we have:

$$\begin{aligned}
 U_{mag} &= U_{mag}^I + U_{mag}^{II} \\
 &= \frac{ab}{2} \int_{-1}^1 \left[ \frac{D_{11}}{a^4} I_1 \left( \frac{d^2 \phi}{d\xi^2} \right)^2 + \frac{2D_{12}}{a^2 b^2} I_2 \frac{d^2 \phi}{d\xi^2} \phi + \frac{D_{22}}{b^4} I_4 \phi^2 \right. \\
 &\quad \left. + \frac{4D_{66}}{a^2 b^2} I_3 \left( \frac{d\phi}{d\xi} \right)^2 \right] d\xi + ab I_1 \left[ \frac{k_{\xi=-1}^r}{a^3} \left( \frac{d\phi}{d\xi} \right)^2 + \frac{k_{\xi=-1}^v}{a} (\phi)^2 \right]_{\xi=-1} \\
 &\quad + ab I_1 \left[ \frac{k_{\xi=1}^r}{a^3} \left( \frac{d\phi}{d\xi} \right)^2 + \frac{k_{\xi=1}^v}{a} (\phi)^2 \right]_{\xi=1},
 \end{aligned}
 \tag{13}$$

123 where the integral parameters are defined as:

$$\begin{aligned}
 I_1 &= \int_{-1}^1 \psi^2 d\eta, \\
 I_2 &= \int_{-1}^1 \left( \frac{d^2 \psi}{d\eta^2} \psi \right) d\eta, \\
 I_3 &= \int_{-1}^1 \left( \frac{d\psi}{d\eta} \right)^2 d\eta, \\
 I_4 &= \int_{-1}^1 \left( \frac{d^2 \psi}{d\eta^2} \right)^2 d\eta.
 \end{aligned}
 \tag{14}$$

124 By taking Equation (8) into account, the coefficient  $T_0$  of the kinetic energy  
 125 from Equation (7) for the plate can be expressed as:

$$T_0 = \frac{ab}{2} \rho h \iint w^2 d\xi d\eta = \frac{ab}{2} \rho h I_1 \int_{-1}^1 \phi^2 d\xi. \quad (15)$$

126 Take the Rayleigh principle in the form:

$$\delta U_{mag} = \omega_x^2 \delta T_0. \quad (16)$$

127 By substituting Equations (13) and (15) into Equation (16), and relieving  
 128  $\delta\phi$  and  $\delta \frac{d\phi}{d\xi}$  in Equation (16) by variation calculus, yields:

$$\begin{aligned} 0 = & \int_{-1}^1 \left[ \frac{D_{11}}{a^4} I_1 \frac{d^4\phi}{d\xi^4} + \left( \frac{2D_{12}}{a^2b^2} I_2 - \frac{4D_{66}}{a^2b^2} I_3 \right) \frac{d^2\phi}{d\xi^2} \right. \\ & + \left. \left( \frac{D_{22}}{b^4} I_4 - \omega_x^2 \rho h I_1 \right) \phi \right] \delta\phi d\xi \\ & + \frac{2k_{\xi=-1}^v}{a} I_1 (\phi \delta\phi)_{\xi=-1} + \frac{2k_{\xi=1}^v}{a} I_1 (\phi \delta\phi)_{\xi=1} \\ & + \left[ \left( \frac{4D_{66}}{a^2b^2} I_3 - \frac{D_{12}}{a^2b^2} I_2 \right) \frac{d\phi}{d\xi} - \frac{D_{11}}{a^4} I_1 \frac{d^3\phi}{d\xi^3} \right] \delta\phi \Big|_{\xi=-1}^{\xi=1} \\ & + \left( \frac{D_{12}}{a^2b^2} I_2 \phi + \frac{D_{11}}{a^4} I_1 \frac{d^2\phi}{d\xi^2} \right) \delta \frac{d\phi}{d\xi} \Big|_{\xi=-1}^{\xi=1} \\ & + \frac{2k_{\xi=-1}^r}{a^3} I_1 \left( \frac{d\phi}{d\xi} \delta \frac{d\phi}{d\xi} \right)_{\xi=-1} + \frac{2k_{\xi=1}^r}{a^3} I_1 \left( \frac{d\phi}{d\xi} \delta \frac{d\phi}{d\xi} \right)_{\xi=1}. \end{aligned} \quad (17)$$

129 Thus, the governing differential equation in the  $x$ -direction can be obtained  
 130 from the integration part in Equation (17):

$$\frac{d^4\phi}{d\xi^4} + 2\alpha^2 \left( \frac{D_{12}I_2}{D_{11}I_1} - 2\frac{D_{66}I_3}{D_{11}I_1} \right) \frac{d^2\phi}{d\xi^2} + \left( \alpha^4 \frac{D_{22}I_4}{D_{11}I_1} - a^4 \Omega_x^4 \right) \phi = 0, \quad (18)$$

131 where  $\Omega_x = \sqrt[4]{\omega_x^2 \rho h / D_{11}}$ . By substituting  $\phi(\xi) = Ae^{\mu\xi}$  into Equation (18),  
 132 yields:

$$\mu^4 + 2\alpha^2 \left( \frac{D_{12}I_2}{D_{11}I_1} - 2\frac{D_{66}I_3}{D_{11}I_1} \right) \mu^2 + \left( \alpha^4 \frac{D_{22}I_4}{D_{11}I_1} - a^4 \Omega_x^4 \right) = 0. \quad (19)$$

133 The solution for  $\mu$  can be expressed as:

$$\mu_{1,2} = \pm i\alpha_1, \quad \mu_{3,4} = \pm \beta_1, \quad (20)$$



134 where,

$$\alpha_1 = \alpha \sqrt{\sqrt{\left(\frac{D_{12}I_2}{D_{11}I_1} - 2\frac{D_{66}I_3}{D_{11}I_1}\right)^2 - \frac{D_{22}I_4}{D_{11}I_1} + b^4\Omega_x^4} + \frac{D_{12}I_2}{D_{11}I_1} - 2\frac{D_{66}I_3}{D_{11}I_1}}, \quad (21a)$$

$$\beta_1 = \alpha \sqrt{\sqrt{\left(\frac{D_{12}I_2}{D_{11}I_1} - 2\frac{D_{66}I_3}{D_{11}I_1}\right)^2 - \frac{D_{22}I_4}{D_{11}I_1} + b^4\Omega_x^4} - \frac{D_{12}I_2}{D_{11}I_1} + 2\frac{D_{66}I_3}{D_{11}I_1}}. \quad (21b)$$

135 The boundary conditions along the edges in the  $x$ -direction can be obtained  
 136 from the remaining  $\delta\phi$  and  $\delta\frac{d\phi}{d\xi}$  parts in Equation (17). The shear force  
 137 equilibrium can be obtained from the  $\delta\phi$  part:

$$\begin{aligned} & \left[ \left( \frac{4D_{66}}{a^2b^2} I_3 - \frac{D_{12}}{a^2b^2} I_2 \right) \frac{d\phi}{d\xi} - \frac{D_{11}}{a^4} I_1 \frac{d^3\phi}{d\xi^3} \right] \Big|_{\xi=-1}^{\xi=1} \\ & + \frac{2k_{\xi=-1}^v}{a} I_1 (\phi)_{\xi=-1} + \frac{2k_{\xi=1}^v}{a} I_1 (\phi)_{\xi=1} = 0, \end{aligned} \quad (22)$$

138 and from the  $\delta\frac{d\phi}{d\xi}$  part, the bending moment equilibrium:

$$\begin{aligned} & \left( \frac{D_{12}}{a^2b^2} I_2 \phi + \frac{D_{11}}{a^4} I_1 \frac{\partial^2 \phi}{\partial \xi^2} \right) \Big|_{\xi=-1}^{\xi=1} + \frac{2k_{\xi=-1}^r}{a^3} I_1 \left( \frac{\partial \phi}{\partial \xi} \right)_{\xi=-1} \\ & \frac{2k_{\xi=1}^r}{a^3} I_1 \left( \frac{\partial \phi}{\partial \xi} \right)_{\xi=1} = 0. \end{aligned} \quad (23)$$

139 Thus, we can obtain the shear force and bending moment equilibrium along  
 140 the edges  $\xi = -1$  and  $\xi = 1$  from Equations (22) and (23), respectively, as:

$$\frac{d^3\phi}{d\xi^3} - \alpha^2 \left( \frac{4D_{66}I_3}{D_{11}I_1} - \frac{D_{12}I_2}{D_{11}I_1} \right) \frac{d\phi}{d\xi} + \frac{2a^3k_{\xi=-1}^v}{D_{11}} \phi = 0, \quad \xi = -1, \quad (24a)$$

$$\frac{d^2\phi}{d\xi^2} + \frac{\alpha^2 D_{12}I_2}{D_{11}I_1} \phi - \frac{2ak_{\xi=-1}^r}{D_{11}} \frac{d\phi}{d\xi} = 0, \quad \xi = -1, \quad (24b)$$

$$\frac{d^3\phi}{d\xi^3} - \alpha^2 \left( \frac{4D_{66}I_3}{D_{11}I_1} - \frac{D_{12}I_2}{D_{11}I_1} \right) \frac{d\phi}{d\xi} - \frac{2a^3k_{\xi=1}^v}{D_{11}} \phi = 0, \quad \xi = 1, \quad (24c)$$

$$\frac{d^2\phi}{d\xi^2} + \frac{\alpha^2 D_{12}I_2}{D_{11}I_1} \phi + \frac{2ak_{\xi=1}^r}{D_{11}} \frac{d\phi}{d\xi} = 0, \quad \xi = 1. \quad (24d)$$

141 Substituting Equation (9a) into Equation (24), and denoting  $k_{\xi}^{v*} = \frac{2a^3k_{\xi}^v}{D_{11}}$ ,  
 142  $k_{\xi}^{r*} = \frac{2ak_{\xi}^r}{D_{11}}$ ,  $S_{\alpha_1} = \sin \alpha_1$ ,  $C_{\alpha_1} = \cos \alpha_1$ ,  $Sh_{\alpha_1} = \sinh \alpha_1$ ,  $Ch_{\alpha_1} = \cosh \alpha_1$ ,

143  $S_{\beta_1} = \sin \beta_1$ ,  $C_{\beta_1} = \cos \beta_1$ ,  $Sh_{\beta_1} = \sinh \beta_1$ , and  $Ch_{\beta_1} = \cosh \beta_1$ , we have:

$$\begin{bmatrix} \gamma_1 C_{\alpha_1} - k_{\xi=-1}^{v*} S_{\alpha_1} & \gamma_1 S_{\alpha_1} + k_{\xi=-1}^{v*} C_{\alpha_1} & \gamma_2 Ch_{\beta_1} - k_{\xi=-1}^{v*} Sh_{\beta_1} \\ \gamma_3 S_{\alpha_1} + k_{\xi=-1}^{r*} \alpha_1 C_{\alpha_1} & -\gamma_3 C_{\alpha_1} + k_{\xi=-1}^{r*} \alpha_1 S_{\alpha_1} & \gamma_4 Sh_{\beta_1} + k_{\xi=-1}^{r*} \beta_1 Ch_{\beta_1} \\ -\gamma_1 C_{\alpha_1} + k_{\xi=1}^{v*} S_{\alpha_1} & \gamma_1 S_{\alpha_1} + k_{\xi=1}^{v*} C_{\alpha_1} & -\gamma_2 Ch_{\beta_1} + k_{\xi=1}^{v*} Sh_{\beta_1} \\ \gamma_3 S_{\alpha_1} + k_{\xi=1}^{r*} \alpha_1 C_{\alpha_1} & \gamma_3 C_{\alpha_1} - k_{\xi=1}^{r*} \alpha_1 S_{\alpha_1} & \gamma_4 Sh_{\beta_1} + k_{\xi=1}^{r*} \beta_1 Ch_{\beta_1} \\ -\gamma_2 Sh_{\beta_1} + k_{\xi=-1}^{v*} Ch_{\beta_1} \\ -\gamma_4 Ch_{\beta_1} - k_{\xi=-1}^{r*} \beta_1 Sh_{\beta_1} \\ -\gamma_2 Sh_{\beta_1} + k_{\xi=1}^{v*} Ch_{\beta_1} \\ \gamma_4 Ch_{\beta_1} + k_{\xi=1}^{r*} \beta_1 Sh_{\beta_1} \end{bmatrix} \begin{Bmatrix} A_1 \\ A_2 \\ A_3 \\ A_4 \end{Bmatrix} = \begin{Bmatrix} 0 \\ 0 \\ 0 \\ 0 \end{Bmatrix}, \quad (25)$$

144 OR,

$$\mathbf{R}_x \mathbf{A} = \mathbf{0}, \quad (26)$$

145 where,

$$\begin{aligned} \gamma_1 &= -\alpha_1^3 - \alpha^2 \left( \frac{4D_{66}S_3}{D_{11}I_1} - \frac{D_{12}I_2}{D_{11}I_1} \right) \alpha_1, \\ \gamma_2 &= \beta_1^3 - \alpha^2 \left( \frac{4D_{66}S_3}{D_{11}I_1} - \frac{D_{12}I_2}{D_{11}I_1} \right) \beta_1, \\ \gamma_3 &= -\alpha_1^2 + \frac{\alpha^2 D_{12}I_2}{D_{11}I_1}, \\ \gamma_4 &= \beta_1^2 + \frac{\alpha^2 D_{12}I_2}{D_{11}I_1}. \end{aligned} \quad (27)$$

146 Note that the classic boundary conditions can be obtained by selecting ex-  
147 tremely large or small spring stiffness constants. For non-trivial solutions,  
148 the characteristic equation or eigenvalue equation is obtained from the de-  
149 terminant of the matrix  $\mathbf{R}_x$  in Equation (26), which must be zero. However,  
150 solving these transcendental equations are cunmbersome and tedious, thus  
151 the DSM is introduced to avoid the ineffective computation.

152 To develop its dynamic stiffness matrix, with the help of Equation (9a),  
153 the vertical displacement and rotation corresponding to the mode shape  $\phi(\xi)$   
154 along the  $x$ -direction at edges  $\xi = -1$  and  $\xi = 1$  can be expressed as:

$$\begin{Bmatrix} \phi_{\xi=-1} \\ \frac{d\phi}{d\xi}_{\xi=-1} \\ \phi_{\xi=1} \\ \frac{d\phi}{d\xi}_{\xi=1} \end{Bmatrix} = \begin{bmatrix} -S_{\alpha_1} & C_{\alpha_1} & -Sh_{\beta_1} & Ch_{\beta_1} \\ \alpha_1 C_{\alpha_1}/a & \alpha_1 S_{\alpha_1}/a & \beta_1 Ch_{\beta_1}/a & -\beta_1 Sh_{\beta_1}/a \\ S_{\alpha_1} & C_{\alpha_1} & Sh_{\beta_1} & Ch_{\beta_1} \\ \alpha_1 C_{\alpha_1}/a & -\alpha_1 S_{\alpha_1}/a & \beta_1 Ch_{\beta_1}/a & \beta_1 Sh_{\beta_1}/a \end{bmatrix} \begin{Bmatrix} A_1 \\ A_2 \\ A_3 \\ A_4 \end{Bmatrix}, \quad (28)$$

155 or,

$$\delta_x = \mathbf{Q}_x \mathbf{A}. \quad (29)$$

156 Note that the eigenvector  $\mathbf{A}$  can be expressed by multiplying the inverse  
 157 matrix  $\mathbf{Q}_x^{-1}$  on the left side of Equation (29), and then substituting  $\mathbf{A}$  into  
 158 Equation (26), we obtain:

$$\mathbf{R}_x \mathbf{A} = \mathbf{R}_x \mathbf{Q}_x^{-1} \delta_x = \mathbf{0}. \quad (30)$$

159 where the dynamic stiffness matrix, denoted as  $\mathbf{K}_x = \mathbf{R}_x \mathbf{Q}_x^{-1}$ , can be ob-  
 160 tained from Equation (30). This matrix can be used to compute the natural  
 161 frequencies of the system instead of solving the eigenvalue equation, and the  
 162 method for the computation will be given in Section 3.

## 163 2.2. Dynamic stiffness matrix corresponding to $\omega_y$

164 In this section, the mode shape  $\phi(\xi)$  derived in *Section 2.1* is utilized to  
 165 obtain the dynamic stiffness matrix in the  $y$ -direction. The vertical trans-  
 166 lational and rotational springs at  $\eta = -1$  are denoted as  $k_{\eta=-1}^v$  and  $k_{\eta=-1}^r$ ,  
 167 respectively, while those at  $\eta = 1$  are represented by  $k_{\eta=1}^v$  and  $k_{\eta=1}^r$ .

168 The magnitude of total potential energy along the edges in the  $y$ -direction  
 169 is given by:

$$\begin{aligned} U_{mag}^{III} = & ab \int \left[ \frac{k_{\eta=-1}^r}{a^3} \left( \frac{\partial w}{\partial \eta} \right)^2 + \frac{k_{\eta=-1}^v}{a} w^2 \right]_{\eta=-1} d\xi \\ & + ab \int \left[ \frac{k_{\eta=1}^r}{a^3} \left( \frac{\partial w}{\partial \eta} \right)^2 + \frac{k_{\eta=1}^v}{a} w^2 \right]_{\eta=1} d\xi. \end{aligned} \quad (31)$$

170 The magnitude of potential energy of the plate in the  $y$ -direction can be  
 171 obtained from Equations (6) and (31) as:

$$\begin{aligned} U_{mag} = & U_{mag}^I + U_{mag}^{III} \\ = & \frac{ab}{2} \iint \left[ \frac{D_{11}}{a^4} \left( \frac{\partial^2 w}{\partial \xi^2} \right)^2 + \frac{2D_{12}}{a^2 b^2} \frac{\partial^2 w}{\partial \xi^2} \frac{\partial^2 w}{\partial \eta^2} + \frac{D_{22}}{b^4} \left( \frac{\partial^2 w}{\partial \eta^2} \right)^2 \right. \\ & \left. + \frac{4D_{66}}{a^2 b^2} \left( \frac{\partial^2 w}{\partial \xi \partial \eta} \right)^2 \right] d\xi d\eta + ab \int \left[ \frac{k_{\eta=1}^r}{b^3} \left( \frac{\partial w}{\partial \eta} \right)^2 + \frac{k_{\eta=1}^v}{b} (w)^2 \right]_{\eta=1} d\xi \\ & + ab \int \left[ \frac{k_{\eta=-1}^r}{b^3} \left( \frac{\partial w}{\partial \eta} \right)^2 + \frac{k_{\eta=-1}^v}{b} (w)^2 \right]_{\eta=-1} d\xi. \end{aligned} \quad (32)$$

172 By substituting Equation (8) into Equation (32), we obtain:

$$\begin{aligned}
U_{mag} &= U_{mag}^I + U_{mag}^{III} \\
&= \frac{ab}{2} \int_{-1}^1 \left[ \frac{D_{11}}{a^4} J_4 \psi^2 + \frac{2D_{12}}{a^2 b^2} J_2 \frac{d^2 \psi}{d\eta^2} \psi + \frac{D_{22}}{b^4} J_1 \left( \frac{d^2 \psi}{d\eta^2} \right)^2 \right. \\
&\quad \left. + \frac{4D_{66}}{a^2 b^2} J_3 \left( \frac{d\psi}{d\eta} \right)^2 \right] d\eta + ab J_1 \left[ \frac{k_{\eta=1}^r}{b^3} \left( \frac{d\psi}{d\eta} \right)^2 + \frac{k_{\eta=1}^v}{b} (\psi)^2 \right]_{\eta=1} \\
&\quad + ab J_1 \left[ \frac{k_{\eta=-1}^r}{b^3} \left( \frac{d\psi}{d\eta} \right)^2 + \frac{k_{\eta=-1}^v}{b} (\psi)^2 \right]_{\eta=-1}, \tag{33}
\end{aligned}$$

173 where the integral parameters are defined as:

$$\begin{aligned}
J_1 &= \int_{-1}^1 \phi^2 d\xi, \\
J_2 &= \int_{-1}^1 \left( \frac{d^2 \phi}{d\xi^2} \phi \right) d\xi, \\
J_3 &= \int_{-1}^1 \left( \frac{d\phi}{d\xi} \right)^2 d\xi, \\
J_4 &= \int_{-1}^1 \left( \frac{d^2 \phi}{d\xi^2} \right)^2 d\xi. \tag{34}
\end{aligned}$$

174 The coefficient  $T_0$  of the kinetic energy from Equation (7) for the plate can  
175 be expressed as:

$$T_0 = \frac{ab}{2} \rho h J_1 \int_{-1}^1 \psi^2 d\eta. \tag{35}$$

176 Take the Rayleigh principle in the form:

$$\delta U_{mag} = \omega_y^2 \delta T_0. \tag{36}$$

177 By substituting Equations (33) and (35) into Equation (36), and relieving

178  $\delta\psi$  and  $\delta\frac{d\psi}{d\eta}$  in Equation (36) by variation calculus, yields:

$$\begin{aligned}
0 = & \int_{-1}^1 \left[ \frac{D_{22}}{b^4} J_1 \frac{d^4\psi}{d\eta^4} + \left( \frac{2D_{12}}{a^2b^2} J_2 - \frac{4D_{66}}{a^2b^2} J_3 \right) \frac{d^2\psi}{d\eta^2} \right. \\
& + \left. \left( \frac{D_{11}}{a^4} J_4 - \omega_y^2 \rho h J_1 \right) \psi \right] \delta\psi d\eta \\
& + \frac{2k_{\eta=-1}^v}{b} J_1 (\psi \delta\psi)_{\eta=-1} + \frac{2k_{\eta=1}^v}{b} J_1 (\psi \delta\psi)_{\eta=1} \\
& + \left[ \left( \frac{4D_{66}}{a^2b^2} J_3 - \frac{D_{12}}{a^2b^2} J_2 \right) \frac{d\psi}{d\eta} - \frac{D_{22}}{b^4} J_1 \frac{d^3\psi}{d\eta^3} \right] \delta\psi \Big|_{\eta=-1}^{\eta=1} \\
& + \left( \frac{D_{12}}{a^2b^2} J_2 \psi + \frac{D_{22}}{b^4} J_1 \frac{d^2\psi}{d\eta^2} \right) \delta \frac{d\psi}{d\eta} \Big|_{\eta=-1}^{\eta=1} \\
& + \frac{2k_{\eta=-1}^r}{b^3} J_1 \left( \frac{d\psi}{d\eta} \delta \frac{d\psi}{d\eta} \right)_{\eta=-1} + \frac{2k_{\eta=1}^r}{b^3} J_1 \left( \frac{d\psi}{d\eta} \delta \frac{d\psi}{d\eta} \right)_{\eta=1}.
\end{aligned} \tag{37}$$

179 Thus, the governing differential equation in the  $y$ -direction can be obtained  
180 from the integration part in Equation (37):

$$\frac{d^4\psi}{d\eta^4} + \frac{2}{\alpha^2} \left( \frac{D_{12}J_2}{D_{22}J_1} - 2 \frac{D_{66}J_3}{D_{22}J_1} \right) \frac{d^2\psi}{d\eta^2} + \left( \frac{D_{11}J_4}{\alpha^4 D_{22}J_1} - \frac{b^4 D_{11}}{D_{22}} \Omega_y^4 \right) \psi = 0, \tag{38}$$

181 where  $\Omega_y = \sqrt[4]{\omega_y^2 \rho h / D_{11}}$ . By substituting  $\psi(\eta) = Be^{\lambda\eta}$  into Equation (38),  
182 yields:

$$\lambda^4 + \frac{2}{\alpha^2} \left( \frac{D_{12}J_2}{D_{22}J_1} - 2 \frac{D_{66}J_3}{D_{22}J_1} \right) \lambda^2 + \left( \frac{D_{11}J_4}{\alpha^4 D_{22}J_1} - \frac{b^4 D_{11}}{D_{22}} \Omega_y^4 \right) = 0. \tag{39}$$

183 The solution for  $\lambda$  can be expressed as:

$$\lambda_{1,2} = \pm i\alpha_2, \quad \lambda_{3,4} = \pm\beta_2, \tag{40}$$

184 where,

$$\alpha_2 = \frac{1}{\alpha} \sqrt{\sqrt{\left( \frac{D_{12}J_2}{D_{22}J_1} - 2 \frac{D_{66}J_3}{D_{22}J_1} \right)^2 - \frac{D_{11}J_4}{D_{22}J_1} + \frac{a^4 D_{11}}{D_{22}} \Omega_y^4} + \frac{D_{12}J_2}{D_{22}J_1} - 2 \frac{D_{66}J_3}{D_{22}J_1}}, \tag{41a}$$

$$\beta_2 = \frac{1}{\alpha} \sqrt{\sqrt{\left( \frac{D_{12}J_2}{D_{22}J_1} - 2 \frac{D_{66}J_3}{D_{22}J_1} \right)^2 - \frac{D_{11}J_4}{D_{22}J_1} + \frac{a^4 D_{11}}{D_{22}} \Omega_y^4} - \frac{D_{12}J_2}{D_{22}J_1} + 2 \frac{D_{66}J_3}{D_{22}J_1}}. \tag{41b}$$

185 The boundary conditions along the edges in the  $y$ -direction can be obtained  
 186 from the remaining  $\delta\psi$  and  $\delta\frac{d\psi}{d\eta}$  parts in Equation (37). The shear force  
 187 equilibrium can be obtained from the  $\delta\psi$  part:

$$\begin{aligned} & \left[ \left( \frac{4D_{66}}{a^2b^2} J_3 - \frac{D_{12}}{a^2b^2} J_2 \right) \frac{d\psi}{d\eta} - \frac{D_{22}}{b^4} J_1 \frac{d^3\psi}{d\eta^3} \right] \Big|_{\eta=-1}^{\eta=1} \\ & + \frac{2k_{\eta=-1}^v}{b} J_1(\psi)_{\eta=-1} + \frac{2k_{\eta=1}^v}{b} J_1(\psi)_{\eta=1} = 0, \end{aligned} \quad (42)$$

188 and from the  $\delta\frac{d\psi}{d\eta}$  part, the bending moment equilibrium:

$$\begin{aligned} & \left( \frac{D_{12}}{a^2b^2} J_2 \psi + \frac{D_{22}}{b^4} J_1 \frac{d^2\psi}{d\eta^2} \right) \Big|_{\eta=-1}^{\eta=1} + \frac{2k_{\eta=-1}^r}{b^3} J_1 \left( \frac{d\psi}{d\eta} \right)_{\eta=-1} \\ & + \frac{2k_{\eta=1}^r}{b^3} J_1 \left( \frac{d\psi}{d\eta} \right)_{\eta=1} = 0. \end{aligned} \quad (43)$$

189 Thus, we can obtain the shear force and bending moment equilibrium along  
 190 the edges  $\eta = -1$  and  $\eta = 1$  from Equations (42) and (43), respectively, as:

$$\frac{d^3\psi}{d\eta^3} - \left( \frac{4D_{66}J_3}{\alpha^2D_{22}J_1} - \frac{D_{12}J_2}{\alpha^2D_{22}J_1} \right) \frac{d\psi}{d\eta} + \frac{2b^3k_{\eta=-1}^v}{D_{22}} \psi = 0, \quad \eta = -1, \quad (44a)$$

$$\frac{d^2\psi}{d\eta^2} + \frac{D_{12}J_2}{\alpha^2D_{22}J_1} \psi - \frac{2bk_{\eta=-1}^r}{D_{22}} \frac{d\psi}{d\eta} = 0, \quad \eta = -1, \quad (44b)$$

$$\frac{d^3\psi}{d\eta^3} - \left( \frac{4D_{66}J_3}{\alpha^2D_{22}J_1} - \frac{D_{12}J_2}{\alpha^2D_{22}J_1} \right) \frac{d\psi}{d\eta} - \frac{2b^3k_{\eta=1}^v}{D_{22}} \psi = 0, \quad \eta = 1, \quad (44c)$$

$$\frac{d^2\psi}{d\eta^2} + \frac{D_{12}J_2}{\alpha^2D_{22}J_1} \psi + \frac{2bk_{\eta=1}^r}{D_{22}} \frac{d\psi}{d\eta} = 0, \quad \eta = 1. \quad (44d)$$

191 Substituting Equation (9b) into Equation (44) and denoting  $k_{\eta}^{v*} = \frac{2b^3k_{\eta}^v}{D_{22}}$ ,  
 192  $k_{\eta}^{r*} = \frac{2bk_{\eta}^r}{D_{22}}$ ,  $S_{\alpha_2} = \sin \alpha_2$ ,  $C_{\alpha_2} = \cos \alpha_2$ ,  $Sh_{\alpha_2} = \sinh \alpha_2$ ,  $Ch_{\alpha_2} = \cosh \alpha_2$ ,  
 193  $S_{\beta_2} = \sin \beta_2$ ,  $C_{\beta_2} = \cos \beta_2$ ,  $Sh_{\beta_2} = \sinh \beta_2$ , and  $Ch_{\beta_2} = \cosh \beta_2$ , We obtain:

$$\begin{aligned} & \begin{bmatrix} \zeta_1 C_{\alpha_2} - k_{\eta=-1}^{v*} S_{\alpha_2} & \zeta_1 S_{\alpha_2} + k_{\eta=-1}^{v*} C_{\alpha_2} & \zeta_2 Ch_{\beta_2} - k_{\eta=-1}^{v*} Sh_{\beta_2} \\ \zeta_3 S_{\alpha_2} + k_{\eta=-1}^{r*} \alpha_2 C_{\alpha_2} & -\zeta_3 C_{\alpha_2} + k_{\eta=-1}^{r*} \alpha_2 S_{\alpha_2} & \zeta_4 Sh_{\beta_2} + k_{\eta=-1}^{r*} \beta_2 Ch_{\beta_2} \\ -\zeta_1 C_{\alpha_2} + k_{\eta=1}^{v*} S_{\alpha_2} & \zeta_1 S_{\alpha_2} + k_{\eta=1}^{v*} C_{\alpha_2} & -\zeta_2 Ch_{\beta_2} + k_{\eta=1}^{v*} Sh_{\beta_2} \\ \zeta_3 S_{\alpha_2} + k_{\eta=1}^{r*} \alpha_2 C_{\alpha_2} & \zeta_3 C_{\alpha_2} - k_{\eta=1}^{r*} \alpha_2 S_{\alpha_2} & \zeta_4 Sh_{\beta_2} + k_{\eta=1}^{r*} \beta_2 Ch_{\beta_2} \\ -\zeta_2 Sh_{\beta_2} + k_{\eta=-1}^{v*} Ch_{\beta_2} & -\zeta_4 Ch_{\beta_2} - k_{\eta=-1}^{r*} \beta_2 Sh_{\beta_2} & \\ -\zeta_2 Sh_{\beta_2} + k_{\eta=1}^{v*} Ch_{\beta_2} & \zeta_4 Ch_{\beta_2} + k_{\eta=1}^{r*} \beta_2 Sh_{\beta_2} & \end{bmatrix} \begin{Bmatrix} B_1 \\ B_2 \\ B_3 \\ B_4 \end{Bmatrix} = \begin{Bmatrix} 0 \\ 0 \\ 0 \\ 0 \end{Bmatrix}, \end{aligned} \quad (45)$$

194 OR,

$$\mathbf{R}_y \mathbf{B} = \mathbf{0}, \quad (46)$$

195 where,

$$\begin{aligned} \zeta_1 &= -\alpha_2^3 - \left( \frac{4D_{66}J_3}{\alpha^2 D_{22}J_1} - \frac{D_{12}J_2}{\alpha^2 D_{22}J_1} \right) \alpha_2, \\ \zeta_2 &= \beta_2^3 - \left( \frac{4D_{66}T_3}{\alpha^2 D_{22}J_1} - \frac{D_{12}J_2}{\alpha^2 D_{22}J_1} \right) \beta_2, \\ \zeta_3 &= -\alpha_2^2 + \frac{D_{12}J_2}{\alpha^2 D_{22}J_1}, \\ \zeta_4 &= \beta_2^2 + \frac{D_{12}J_2}{\alpha^2 D_{22}J_1}. \end{aligned} \quad (47)$$

196 With the help of Equation (9b), the vertical displacement and rotation cor-  
197 responding to the mode shape  $\psi$  along the  $y$ -direction at the edges  $\eta = -1$   
198 and  $\eta = 1$  can be expressed as:

$$\begin{Bmatrix} \psi_{\eta=-1} \\ \frac{d\psi}{d\eta}_{\eta=-1} \\ \psi_{\eta=1} \\ \frac{d\psi}{d\eta}_{\eta=1} \end{Bmatrix} = \begin{bmatrix} -S_{\alpha_2} & C_{\alpha_2} & -Sh_{\beta_2} & Ch_{\beta_2} \\ \frac{\alpha_2 C_{\alpha_2}}{b} & \frac{\alpha_2 S_{\alpha_2}}{b} & \frac{\beta_2 Ch_{\beta_2}}{b} & -\frac{\beta_2 Sh_{\beta_2}}{b} \\ S_{\alpha_2} & C_{\alpha_2} & Sh_{\beta_2} & Ch_{\beta_2} \\ \frac{\alpha_2 C_{\alpha_2}}{b} & -\frac{\alpha_2 S_{\alpha_2}}{b} & \frac{\beta_2 Ch_{\beta_2}}{b} & \frac{\beta_2 Sh_{\beta_2}}{b} \end{bmatrix} \begin{Bmatrix} B_1 \\ B_2 \\ B_3 \\ B_4 \end{Bmatrix}, \quad (48)$$

199 OR,

$$\delta_y = \mathbf{Q}_y \mathbf{B}. \quad (49)$$

200 Note that the eigenvector  $\mathbf{B}$  can be expressed by multiplying the inverse  
201 matrix  $\mathbf{Q}_y^{-1}$  on the left-hand side of Equation (49), and then substituting  $\mathbf{B}$   
202 into Equation (46), we obtain:

$$\mathbf{R}_y \mathbf{B} = \mathbf{R}_y \mathbf{Q}_y^{-1} \delta_y = \mathbf{0}, \quad (50)$$

203 where the dynamic stiffness matrix, denoted as  $\mathbf{K}_y = \mathbf{R}_y \mathbf{Q}_y^{-1}$ , can be ob-  
204 tained from Equation (50).

### 205 3. Frequency and mode shape computation

#### 206 3.1. Wittrick-Williams algorithm and enhancement

207 The Wittrick-Williams (W-W) algorithm [23] is an effective method for  
208 determining the natural frequencies from the dynamic stiffness matrix with

209 high reliability. Instead of directly solving the equations, the algorithm com-  
 210 putes the total number  $J$  of natural frequencies below a given frequency  $\omega^*$ ,  
 211 which is represented as:

$$J(\omega^*) = J_0(\omega^*) + s\{\mathbf{K}^\Delta(\omega^*)\} = J_0(\omega^*) + J_k(\omega^*), \quad (51)$$

212 where  $J_0$  represents the number of natural frequencies of the structure with  
 213 all ends fully clamped,  $\mathbf{K}^\Delta$  is the upper triangular matrix obtained from the  
 214 dynamic stiffness matrix  $\mathbf{K}$  after applying Gaussian elimination, and  $J_k(\omega^*)$   
 215 denotes the number of negative elements in the leading diagonal of  $\mathbf{K}^\Delta$ .

216 It should be noted that the  $J_0$  count is a crucial aspect when applying the  
 217 W-W algorithm. Many previous studies use a sufficiently fine mesh or enough  
 218 terms in series expansions to capture all fully clamped natural frequencies,  
 219 ensuring computational accuracy [1]. However, this approach can make the  
 220 application process cumbersome. To address this issue, the fully clamped  
 221 problem can be replaced with a simply supported problem, where the Navier  
 222 solution for the simply supported plate is used to count  $J_0$  [18]. Nevertheless,  
 223 since analytical solutions in DSM methods involve an infinite series of Fourier  
 224 terms, a sufficient number of truncation terms is required to ensure accuracy  
 225 and convergence.

226 In fact,  $J_0$  can be indirectly determined by evaluating the number of  
 227 natural frequencies  $J$  of the structure under specific boundary conditions,  
 228 which are generally different from the original boundary conditions [8]:

$$J_0(p_1, \omega^*) = J(\bar{p}_1, \omega^*) - J_k(\bar{p}_1, \omega^*), \quad (52)$$

229 where  $p_1$  denotes the fully clamped supports, and  $\bar{p}_1$  denotes specific sup-  
 230 ports, which are typically simply supported, guided, or a combination of the  
 231 two. For these specific boundary conditions, the eigenvalue equations of SOV  
 232 type solution take the form of a single harmonic function. By substituting  
 233 Equation (52) into Equation (51) we get the algorithm as:

$$J(p, \omega^*) = J(\bar{p}_1, \omega^*) - J_k(\bar{p}_1, \omega^*) + J_k(p, \omega^*) \quad (53)$$

234 where  $p$  represents the original boundary conditions of the structure. There-  
 235 fore, the challenge of determining  $J_0(p_1, \omega^*)$  can be transformed into the  
 236 problem of solving  $J(\bar{p}_1, \omega^*)$  instead. By considering fully simply supported  
 237 boundary conditions, the eigenvalue equation corresponding to the natural



frequency parameter  $\Omega_x$  can be obtained from the determinant of the coefficient matrix  $\mathbf{R}_x$  in Equation (25), as given by:

$$\sin 2\alpha_1 = 0. \quad (54)$$

With the help of Equations (21a) and (54), the closed-form solution of the  $n_x$ -th simply supported frequency  $\Omega_{x,n_x}$  for the given  $n_y$ -order  $\psi_{n_y}(\eta)$  can be expressed as:

$$\Omega_{x,n_x} = \frac{1}{b} \sqrt[4]{\left[ \left( \frac{n_x \pi}{2\alpha} \right)^2 - \frac{D_{12}S_2}{D_{11}S_1} + 2\frac{D_{66}S_3}{D_{11}S_1} \right]^2 - \left( \frac{D_{12}S_2}{D_{11}S_1} - 2\frac{D_{66}S_3}{D_{11}S_1} \right)^2 + \frac{D_{22}S_4}{D_{11}S_1}}. \quad (55)$$

For  $\Omega_{x,n_x} \leq \Omega_x^* < \Omega_{x,n_x+1}$ ,  $J(\bar{p}_1, \Omega_x^*) = n_x$ . Similarly, the closed-form solution of the  $n_y$ -th simply supported frequency  $\Omega_{y,n_y}$  for the given  $n_x$ -order  $\phi_{n_x}(\xi)$  can be expressed as:

$$\Omega_{y,n_y} = \frac{1}{a} \sqrt[4]{\frac{D_{22}}{D_{11}} \left\{ \left[ \left( \frac{n_y \pi \alpha}{2} \right)^2 - \frac{D_{12}T_2}{D_{22}T_1} + 2\frac{D_{66}T_3}{D_{22}T_1} \right]^2 - \left( \frac{D_{12}T_2}{D_{22}T_1} - 2\frac{D_{66}T_3}{D_{22}T_1} \right)^2 + \frac{D_{11}T_4}{D_{22}T_1} \right\}}. \quad (56)$$

For  $\Omega_{y,n_y} \leq \Omega_y^* < \Omega_{y,n_y+1}$ ,  $J(\bar{p}_1, \Omega_y^*) = n_y$ . According to the relationships  $\Omega_x = \sqrt[4]{\omega_x^2 \rho h / D_{11}}$  and  $\Omega_y = \sqrt[4]{\omega_y^2 \rho h / D_{11}}$ , the values of  $J(\bar{p}_1, \omega_x^*)$  and  $J(\bar{p}_1, \omega_y^*)$  can be derived from  $J(\bar{p}_1, \Omega_x^*)$  and  $J(\bar{p}_1, \Omega_y^*)$ , respectively. Therefore, this refined W-W algorithm can be applied to estimate the lower and upper bounds of the frequency range, denoted as  $\omega_l$  and  $\omega_u$ , yielding an approximation for the frequency  $\omega_a \in (\omega_l, \omega_u)$ .

### 3.2. Mode shape computation

The mode shape coefficients  $A_1$  to  $A_4$  and  $B_1$  to  $B_4$  in the eigenvectors  $\mathbf{A}$  and  $\mathbf{B}$  for all classic boundary conditions are provided in [27]. Alternatively, these coefficients can also be obtained through a simple numerical method, which this work presents as an approach. Here, we illustrate solving the eigenvector  $\mathbf{A}$  as an example. By assuming the exact natural frequency as

258  $\omega_k$ , we can expand the coefficient matrix  $\mathbf{R}_x$  in Equation (25) using a first-  
 259 order Taylor series about  $\omega_a$ :

$$\mathbf{R}_{x,k}(\omega_k)\mathbf{A}_k = \mathbf{R}_{x,a}\mathbf{A}_k + (\omega_k - \omega_a)\mathbf{R}'_{x,a}\mathbf{A}_k + O((\omega_k - \omega_a)^2) = 0. \quad (57)$$

260 Ignoring higher-order terms, an eigenvalue problem can be derived from  
 261 Equation (57):

$$(\mathbf{R}'_{x,a})^{-1}\mathbf{R}_{x,a}\mathbf{A} = (\omega_a - \omega_k)\mathbf{A} = \tau\mathbf{A}. \quad (58)$$

262 This eigenvalue problem can be solved using the inverse iteration procedure  
 263 [30]:

$$\bar{\mathbf{A}}^{(i+1)} = \mathbf{R}_{x,a}^{-1}\mathbf{R}'_{x,a}\mathbf{A}^{(i)}, \quad (59)$$

264 where the initial guess for  $\mathbf{A}^{(0)}$  is a column vector consisting of four randomly  
 265 generated elements, each of which falls within the range (0,1). The updated  
 266 eigenvalue for the next step can be obtained as:

$$\tau^{(i+1)} = \frac{1}{\bar{A}_j^{(i+1)}}, \quad (60)$$

267 where,

$$|\bar{A}_j^{(i+1)}| = \max(|\bar{A}_1^{(i+1)}|, |\bar{A}_2^{(i+1)}|, |\bar{A}_3^{(i+1)}|, |\bar{A}_4^{(i+1)}|). \quad (61)$$

268 The updated eigenvector can be obtained as:

$$\mathbf{A}^{(i+1)} = \tau^{(i+1)}\bar{\mathbf{A}}^{(i+1)}. \quad (62)$$

269 The procedure can be controlled by the error tolerance  $\epsilon$  or maximum allowed  
 270 steps  $i_{\max}$ :

$$\max |A_n^{(i+1)} - A_n^{(i)}| < \epsilon, \quad (63a)$$

$$i = i_{\max}. \quad (63b)$$

271 Note that the mode shape coefficients  $A_1$  to  $A_4$  obtained from  $\mathbf{A}^{(i+1)}$  are  
 272 applied for the elastically restrained boundary conditions.

### 273 3.3. Application procedure

274 The procedure of the proposed method is as follows:

- 275 • **Step 1** Assume initial integral parameters  $I_1^{(0)}, I_2^{(0)}, I_3^{(0)}$ , and  $I_4^{(0)}$  in the  
 276  $y$ -direction. Using the given boundary conditions at  $\xi = -1$  and  $\xi = 1$ ,  
 277 determine  $\mathbf{K}_x^{(0)}$  from Equation (30). Then, apply the computational  
 278 algorithms in Section 3.1 to compute the lower and upper bounds of the  
 279  $n_x$ -th non-dimensional frequency parameter,  $2a\Omega_{l,x,n_x}^{(0)}$  and  $2a\Omega_{u,x,n_x}^{(0)}$ ,  
 280 and take the average  $2a\Omega_{x,n_x}^{(0)} = (2a\Omega_{l,x,n_x}^{(0)} + 2a\Omega_{u,x,n_x}^{(0)})/2$  along with its  
 281 corresponding mode shape  $\phi_{n_x}^{(0)}$ , where  $n_x = 1, 2, 3, \dots$
- 282 • **Step 2** Use  $\phi_{n_x}^{(0)}$  as the prescribed mode to determine  $\mathbf{K}_y^{(1)}$  in Equa-  
 283 tion (50), considering the boundary conditions at  $\eta = -1$  and  $\eta = 1$ .  
 284 Apply the computational algorithms to obtain the  $n_y$ -th frequency pa-  
 285 rameter  $2a\Omega_{y,n_y}^{(1)}$  and its corresponding mode shape  $\psi_{n_y}^{(1)}$ , where  $n_y =$   
 286  $1, 2, 3, \dots$ . This completes the first iteration cycle.
- 287 • **Step 3** Use  $\psi_{n_y}^{(1)}$  as the prescribed  $n_y$ -th mode shape in the  $y$ -direction to  
 288 compute  $\mathbf{K}_x^{(1)}$  from Equation (30), then determine the  $n_x$ -th frequency  
 289 parameter  $2a\Omega_{x,n_x}^{(1)}$  and its corresponding mode shape  $\phi_{n_x}^{(1)}$ .
- 290 • **Step 4** Use  $\phi_{n_x}^{(1)}$  as the prescribed mode in the  $x$ -direction to com-  
 291 pute the  $n_y$ -th frequency parameter  $2a\Omega_{y,n_y}^{(2)}$  and its corresponding mode  
 292 shape  $\psi_{n_y}^{(2)}$ , completing the second iteration cycle.
- 293 • **Step 5** Stop the iteration if  $|2a\Omega_{x,n_x}^{(i)} - 2a\Omega_{x,n_x}^{(i+1)}| \leq \Delta 2a\Omega$  or  $|2a\Omega_{y,n_y}^{(i)} -$   
 294  $2a\Omega_{y,n_y}^{(i+1)}| \leq \Delta 2a\Omega$ , where  $\Delta 2a\Omega = 2a\Omega_u - 2a\Omega_l$ . Here,  $2a\Omega_l$  and  $2a\Omega_u$   
 295 are the lower and upper bounds of the frequency parameter range,  
 296 within which the actual frequency parameter  $2a\Omega$  lies, i.e.,  $2a\Omega \in$   
 297  $(2a\Omega_l, 2a\Omega_u)$ . The quantity  $\Delta 2a\Omega$  represents the frequency param-  
 298 eter interval used in the W-W algorithm.
- 299 • **Step 6** Finally, construct the  $(n_x, n_y)$ -th mode shape as  $w(\xi, \eta) =$   
 300  $\phi_{n_x}(\xi)\psi_{n_y}(\eta)$  using Equation (8).

## 301 4. Numerical Results

302 This section presents the numerical validation of the proposed method for  
 303 classic boundary conditions and rotationally restrained boundary conditions.  
 304 For all numerical calculations, the initial integral parameters are assumed  
 305 as  $I_1^{(0)} = 1$ ,  $I_2^{(0)} = 1$ ,  $I_3^{(0)} = 1$ , and  $I_4^{(0)} = 10$  in the  $y$ -direction, serving  
 306 as the starting point of **Step 1** for any mode in all boundary conditions.

307 In this section, the interval between the upper and lower bounds of the  
 308 non-dimensional frequency parameter,  $2a\Delta\Omega$ , is set to 0.005, limiting the  
 309 error range. According to our numerical calculations, two iteration cycles  
 310 are generally sufficient to meet the convergence requirement (i.e.,  $|2a\Omega_x^{(i)} -$   
 311  $2a\Omega_x^{(i+1)}| \leq \Delta 2a\Omega$  or  $|2a\Omega_y^{(i)} - 2a\Omega_y^{(i+1)}| \leq \Delta 2a\Omega$ ) for most cases, with at most  
 312 three cycles required when applying the iterative procedure in Section 3.3.

#### 313 4.1. Classical boundary conditions

314 In this subsection, the proposed method is validated by comparison with  
 315 the extended SOV method [27]. The properties of the orthotropic plate,  
 316 consistent with those in [27], are as follows:  $E_1 = 185\text{GPa}$ ,  $E_2 = 10.5\text{GPa}$ ,  
 317  $G_{12} = 7.3\text{GPa}$ ,  $\rho = 1600 \text{ kg m}^{-3}$ , and  $\nu_{12} = 0.28$ .

318 The translational springs ( $k_\xi^v$ ) and rotational springs ( $k_\xi^r$ ) along all edges  
 319 can be set to zero or infinity (represented as  $1 \times 10^{15} \text{ N m}^{-1}$  in the numerical  
 320 calculations of this study) to obtain different classic boundary conditions.

321 The results for SSSS, SCSF, GCGC, CCCC, SCCC, SCCC, GGCC, CCFF,  
 322 CFCF, CFFF, and FFFF boundary conditions are presented in Tables 1  
 323 to 3. These results demonstrate high accuracy compared to the extended  
 324 SOV method, with difference remaining smaller than the frequency parameter  
 325 interval  $2a\Delta\Omega = 0.005$ . The frequency parameters in both directions are  
 326 equal ( $2a\Omega_x - 2a\Omega_y = 0$ ) in almost all cases, with a few exceptions where  
 327  $2a\Omega_x - 2a\Omega_y = 0.005$ . In fact, higher accuracy compared to the extended  
 328 SOV method can be achieved if the frequency parameter interval  $2a\Delta\Omega$  is set  
 329 smaller than 0.005. It should be noted that the accuracy improves only by  
 330 reducing  $2a\Delta\Omega$ , and no additional iterations are required according to our  
 331 calculations. Figure 2 shows the first six nonzero mode shapes of a square  
 332 orthotropic plate with FFFF boundary conditions, where the mode shape coefficients  
 333 are calculated using the numerical method developed in this study.  
 334 Instead of selecting fixed expressions for the mode shape coefficients based  
 335 on specific boundary conditions, our method is applicable to all boundary  
 336 conditions.

#### 337 4.2. Rotationally restrained boundary conditions

338 In this subsection, rectangular orthotropic plates with rotationally re-  
 339 strained edges ( $k_\xi^v = k_\eta^v = \infty$ ) are validated. The rotational stiffness coefficient

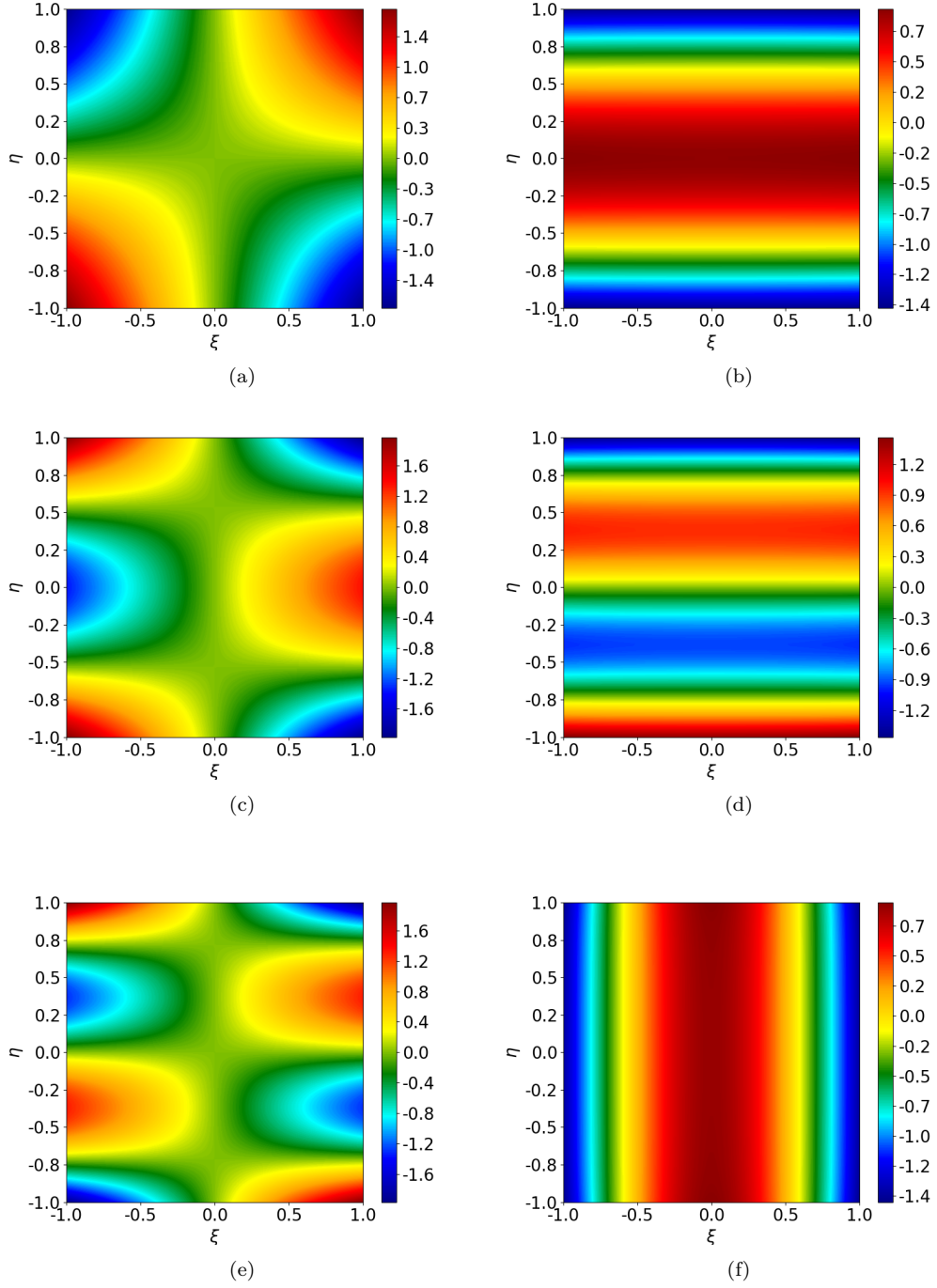


Figure 2: The first six nonzero mode shapes of a square orthotropic plate with FFFF boundary conditions: (a) the first mode; (b) the second mode; (c) the third mode; (d) the fourth mode; (e) the fifth mode; (f) the sixth mode.

Table 1: The first seven frequency parameter  $2a\Omega$  of of orthotropic rectangular plates with SSSS, SCSF and GCGC boundary conditions.

| BCs  | $\alpha$ | Mode            | $2a\Omega_x = 2a\Omega_y = 2a\sqrt{\rho h \omega^2 / D_{11}}$ |        |        |        |        |        |        |
|------|----------|-----------------|---|--------|--------|--------|--------|--------|--------|
|      |          |                 | 1   | 2      | 3      | 4      | 5      | 6      | 7      |
| SSSS | 0.5      | Mode number     | (1,1)   | (1,2)  | (1,3)  | (1,4)  | (1,5)  | (1,6)  | (1,7)  |
|      |          | extended SOV 27 | 3.1807  | 3.3190 | 3.5938 | 4.0135 | 4.5495 | 5.1635 | 5.8265 |
|      |          | Present         | 3.1825  | 3.3225 | 3.5975 | 4.0175 | 4.5525 | 5.1625 | 5.8275 |
|      | 1        | Mode number     | (1,1)   | (1,2)  | (1,3)  | (2,1)  | (1,4)  | (2,2)  | (2,3)  |
|      |          | extended SOV 27 | 3.3190  | 4.0135 | 5.1635 | 6.3615 | 6.5200 | 6.6379 | 7.1876 |
|      |          | Present         | 3.3175  | 4.0175 | 5.1625 | 6.3625 | 6.5175 | 6.6375 | 7.1875 |
|      | 1.5      | Mode number     | (1,1)   | (1,2)  | (2,1)  | (2,2)  | (1,3)  | (2,3)  | (1,4)  |
|      |          | extended SOV 27 | 3.5938  | 5.1635 | 6.4698 | 7.1876 | 7.2331 | 8.5389 | 9.4352 |
|      |          | Present         | 3.5975  | 5.1675 | 6.4725 | 7.1875 | 7.2325 | 8.5375 | 9.4375 |
| SCSF | 0.5      | Mode number     | (1,1)   | (1,2)  | (1,3)  | (1,4)  | (1,5)  | (1,6)  | (1,7)  |
|      |          | extended SOV 27 | 3.1516  | 3.2451 | 3.4588 | 3.8131 | 4.2950 | 4.8711 | 5.5087 |
|      |          | Present         | 3.1525  | 3.2475 | 3.4575 | 3.8175 | 4.2925 | 4.8725 | 5.5075 |
|      | 1        | Mode number     | (1,1)   | (1,2)  | (1,3)  | (1,4)  | (2,1)  | (2,2)  | (2,3)  |
|      |          | extended SOV 27 | 3.1908  | 3.6428 | 4.5972 | 5.8599 | 6.3033 | 6.4901 | 6.9177 |
|      |          | Present         | 3.1925  | 3.6425 | 4.5975 | 5.8575 | 6.3025 | 6.4925 | 6.9175 |
|      | 1.5      | Mode number     | (1,1)   | (1,2)  | (1,3)  | (2,1)  | (2,2)  | (2,3)  | (1,4)  |
|      |          | extended SOV 27 | 3.2710  | 4.3430 | 6.2157 | 6.3337 | 6.8043 | 7.8718 | 8.3518 |
|      |          | Present         | 3.2725  | 4.3425 | 6.2175 | 6.3325 | 6.8025 | 7.8725 | 8.3525 |
| GCGC | 0.5      | Mode number     | (1,1)   | (1,2)  | (1,3)  | (2,1)  | (2,2)  | (1,4)  | (2,3)  |
|      |          | extended SOV 27 | 1.1544  | 1.9166 | 2.6835 | 3.1983 | 3.3890 | 3.4501 | 3.7372 |
|      |          | Present         | 1.1525  | 1.9175 | 2.6825 | 3.1975 | 3.3875 | 3.4525 | 3.7375 |
|      | 1        | Mode number     | (1,1)   | (2,1)  | (1,2)  | (2,2)  | (1,3)  | (2,3)  | (3,1)  |
|      |          | extended SOV 27 | 2.3087  | 3.4900 | 3.8331 | 4.4682 | 5.3669 | 5.7736 | 6.3967 |
|      |          | Present         | 2.3075  | 3.4875 | 3.8325 | 4.4675 | 5.3675 | 5.7725 | 6.3975 |
|      | 1.5      | Mode number     | (1,1)   | (2,1)  | (1,2)  | (2,2)  | (3,1)  | (3,2)  | (1,3)  |
|      |          | extended SOV 27 | 3.4631  | 4.1353 | 5.7497 | 6.0981 | 6.6049 | 7.6449 | 8.0504 |
|      |          | Present         | 3.4625  | 4.1325 | 5.7475 | 6.0975 | 6.6075 | 7.6425 | 8.0525 |

Table 2: The first seven frequency parameter  $2a\Omega$  of of orthotropic rectangular plates with CCCC, SSCC, SCCC and GGCC boundary conditions.

| BCs  | $\alpha$ | Mode            | $2a\Omega_x = 2a\Omega_y = 2a\sqrt{\rho h \omega^2 / D_{11}}$ |        |        |        |        |        |         |
|------|----------|-----------------|---|--------|--------|--------|--------|--------|---------|
|      |          |                 | 1   | 2      | 3      | 4      | 5      | 6      | 7       |
| CCCC | 0.5      | Mode number     | (1,1)   | (1,2)  | (1,3)  | (1,4)  | (1,5)  | (1,6)  | (1,7)   |
|      |          | extended SOV 27 | 4.7500  | 4.8208 | 4.9682 | 5.2177 | 5.5791 | 6.0430 | 6.5892  |
|      |          | Present         | 4.7475  | 4.8225 | 4.9725 | 5.2175 | 5.5825 | 6.0425 | 6.5875  |
|      | 1        | Mode number     | (1,1)   | (1,2)  | (1,3)  | (1,4)  | (2,1)  | (2,2)  | (2,3)   |
|      |          | extended SOV 27 | 4.8579  | 5.3546 | 6.2819 | 7.4972 | 7.9193 | 8.1490 | 8.6054  |
|      |          | Present         | 4.8575  | 5.3575 | 6.2875 | 7.4975 | 7.9175 | 8.1475 | 8.6075  |
|      | 1.5      | Mode number     | (1,1)   | (1,2)  | (2,1)  | (1,3)  | (2,2)  | (2,3)  | (1,4)   |
|      |          | extended SOV 27 | 5.1581  | 6.5412 | 8.0409 | 8.4945 | 8.7204 | 9.9793 | 10.6460 |
|      |          | Present         | 5.1575  | 6.5375 | 8.0425 | 8.4975 | 8.7175 | 9.9775 | 10.6425 |
| SSCC | 0.5      | Mode number     | (1,1)   | (1,2)  | (1,3)  | (1,4)  | (1,5)  | (1,6)  | (1,7)   |
|      |          | extended SOV 27 | 3.9542  | 4.0520 | 4.2525 | 4.5785 | 5.0254 | 5.5682 | 6.1789  |
|      |          | Present         | 3.9575  | 4.0525 | 4.2475 | 4.5775 | 5.0225 | 5.5725 | 6.1825  |
|      | 1        | Mode number     | (1,1)   | (1,2)  | (1,3)  | (1,4)  | (2,1)  | (2,2)  | (2,3)   |
|      |          | extended SOV 27 | 4.0745  | 4.6606 | 5.7009 | 6.9940 | 7.1396 | 7.3894 | 7.8881  |
|      |          | Present         | 4.0775  | 4.6625 | 5.7025 | 6.9925 | 7.1375 | 7.3875 | 7.8875  |
|      | 1.5      | Mode number     | (1,1)   | (1,2)  | (2,1)  | (1,3)  | (2,2)  | (2,3)  | (1,4)   |
|      |          | extended SOV 27 | 4.3602  | 5.8384 | 7.2531 | 7.8560 | 7.9481 | 9.2515 | 10.0366 |
|      |          | Present         | 4.3625  | 5.8325 | 7.2525 | 7.8575 | 7.9525 | 9.2525 | 10.0325 |
| SCCC | 0.5      | Mode number     | (1,1)   | (1,2)  | (1,3)  | (1,4)  | (1,5)  | (1,6)  | (1,7)   |
|      |          | extended SOV 27 | 3.9596  | 4.0745 | 4.3027 | 4.6606 | 5.1361 | 5.7009 | 6.3271  |
|      |          | Present         | 3.9575  | 4.0725 | 4.3025 | 4.6625 | 5.1325 | 5.7025 | 6.3325  |
|      | 1        | Mode number     | (1,1)   | (1,2)  | (1,3)  | (2,1)  | (1,4)  | (2,2)  | (2,3)   |
|      |          | extended SOV 27 | 4.1349  | 4.8478 | 5.9805 | 7.1541 | 7.3192 | 7.4478 | 8.0121  |
|      |          | Present         | 4.1325  | 4.8475 | 5.9825 | 7.1525 | 7.3175 | 7.4475 | 8.0125  |
|      | 1.5      | Mode number     | (1,1)   | (1,2)  | (2,1)  | (2,2)  | (1,3)  | (2,3)  | (3,1)   |
|      |          | extended SOV 27 | 4.5824  | 6.2766 | 7.3116 | 8.1528 | 8.3705 | 9.5986 | 10.3507 |
|      |          | Present         | 4.5825  | 6.2775 | 7.3125 | 8.1525 | 8.3725 | 9.5975 | 10.3525 |
| GGCC | 0.5      | Mode number     | (1,1)   | (1,2)  | (1,3)  | (1,4)  | (1,5)  | (1,6)  | (1,7)   |
|      |          | extended SOV 27 | 2.3750  | 2.4841 | 2.7895 | 3.2946 | 3.9226 | 4.6123 | 5.3326  |
|      |          | Present         | 2.3725  | 2.4875 | 2.7925 | 3.2975 | 3.9225 | 4.6075 | 5.3325  |
|      | 1        | Mode number     | (1,1)   | (1,2)  | (1,3)  | (2,1)  | (2,2)  | (1,4)  | (2,3)   |
|      |          | extended SOV 27 | 2.4290  | 3.1410 | 4.4293 | 5.5202 | 5.7315 | 5.8801 | 6.2606  |
|      |          | Present         | 2.4325  | 3.1425 | 4.4325 | 5.5225 | 5.7325 | 5.8775 | 6.2625  |
|      | 1.5      | Mode number     | (1,1)   | (1,2)  | (2,1)  | (2,2)  | (1,3)  | (2,3)  | (3,1)   |
|      |          | extended SOV 27 | 2.5790  | 4.2472 | 5.5565 | 6.1533 | 6.4347 | 7.5231 | 8.6732  |
|      |          | Present         | 2.5825  | 4.2475 | 5.5575 | 6.1525 | 6.4325 | 7.5225 | 8.6725  |

Table 3: The first seven nonzero frequency parameter  $2a\Omega$  of of orthotropic rectangular plates with CCFF, CFCF, CFFF and FFFF boundary conditions.

| BCs  | $\alpha$ | Mode            | $2a\Omega_x = 2a\Omega_y = 2a\sqrt{\rho h \omega^2 / D_{11}}$ |        |        |        |        |        |        |
|------|----------|-----------------|---|--------|--------|--------|--------|--------|--------|
|      |          |                 | 1   | 2      | 3      | 4      | 5      | 6      | 7      |
| CCFF | 0.5      | Mode number     | (1,1)   | (1,2)  | (1,3)  | (1,4)  | (1,5)  | (1,6)  | (2,1)  |
|      |          | extended SOV 27 | 1.8978  | 2.0905 | 2.4925 | 3.0563 | 3.7110 | 4.4117 | 4.7029 |
|      |          | Present         | 1.8975  | 2.0925 | 2.4925 | 3.0575 | 3.7125 | 4.4125 | 4.7025 |
|      | 1        | Mode number     | (1,1)   | (1,2)  | (1,3)  | (2,1)  | (2,2)  | (1,4)  | (2,3)  |
|      |          | extended SOV 27 | 1.9930  | 2.7895 | 4.0733 | 4.7338 | 5.0652 | 5.5128 | 5.7419 |
|      |          | Present         | 1.9925  | 2.7875 | 4.0725 | 4.7325 | 5.0675 | 5.5125 | 5.7425 |
|      | 1.5      | Mode number     | (1,1)   | (1,2)  | (2,1)  | (2,2)  | (1,3)  | (2,3)  | (3,1)  |
|      |          | extended SOV 27 | 2.1780  | 3.7411 | 4.7931 | 5.5758 | 5.8895 | 7.0263 | 7.9006 |
|      |          | Present         | 2.1775  | 3.7425 | 4.7925 | 5.5725 | 5.8875 | 7.0275 | 7.9025 |
| CFCF | 0.5      | Mode number     | (1,1)   | (1,2)  | (1,3)  | (1,4)  | (1,5)  | (1,6)  | (1,7)  |
|      |          | extended SOV 27 | 4.7297  | 4.7427 | 4.7881 | 4.8819 | 5.0478 | 5.3072 | 5.6694 |
|      |          | Present         | 4.7275  | 4.7425 | 4.7875 | 4.8825 | 5.0475 | 5.3075 | 5.6675 |
|      | 1        | Mode number     | (1,1)   | (1,2)  | (1,3)  | (1,4)  | (1,5)  | (1,6)  | (2,1)  |
|      |          | extended SOV 27 | 4.7295  | 4.7817 | 5.0012 | 5.5348 | 6.4407 | 7.6182 | 7.8523 |
|      |          | Present         | 4.7275  | 4.7825 | 5.0025 | 5.5325 | 6.4425 | 7.6175 | 7.8525 |
|      | 1.5      | Mode number     | (1,1)   | (1,2)  | (1,3)  | (1,4)  | (2,1)  | (2,2)  | (2,3)  |
|      |          | extended SOV 27 | 4.7292  | 4.8458 | 5.4221 | 6.7635 | 7.8518 | 7.9470 | 8.3021 |
|      |          | Present         | 4.7275  | 4.8475 | 5.4225 | 6.7625 | 7.8525 | 7.9475 | 8.3025 |
| CFFF | 0.5      | Mode number     | (1,1)   | (1,2)  | (1,3)  | (1,4)  | (1,5)  | (1,6)  | (1,7)  |
|      |          | extended SOV 27 | 1.8751  | 1.9439 | 2.1679 | 2.5657 | 3.1106 | 3.7486 | 4.4382 |
|      |          | Present         | 1.8775  | 1.9425 | 2.1675 | 2.5675 | 3.1125 | 3.7475 | 4.4375 |
|      | 1        | Mode number     | (1,1)   | (1,2)  | (1,3)  | (1,4)  | (2,1)  | (2,2)  | (2,3)  |
|      |          | extended SOV 27 | 1.8750  | 2.1242 | 2.9077 | 4.1319 | 4.6937 | 4.8226 | 5.2263 |
|      |          | Present         | 1.8775  | 2.1225 | 2.9075 | 4.1325 | 4.6925 | 4.8225 | 5.2275 |
|      | 1.5      | Mode number     | (1,1)   | (1,2)  | (1,3)  | (2,1)  | (2,2)  | (2,3)  | (1,4)  |
|      |          | extended SOV 27 | 1.8750  | 2.3402 | 3.8522 | 4.6935 | 4.9753 | 5.8314 | 5.9292 |
|      |          | Present         | 1.8775  | 2.3425 | 3.8525 | 4.6925 | 4.9775 | 5.8325 | 5.9275 |
| FFFF | 0.5      | Mode number     | (1,3)   | (2,2)  | (1,4)  | (2,3)  | (1,5)  | (2,4)  | (2,5)  |
|      |          | extended SOV 27 | 1.1540  | 1.4858 | 1.9157 | 2.1704 | 2.6821 | 2.7881 | 3.4093 |
|      |          | Present         | 1.1525  | 1.4875 | 1.9175 | 2.1725 | 2.6825 | 2.7875 | 3.4075 |
|      | 1        | Mode number     | (2,2)   | (1,3)  | (2,3)  | (1,4)  | (2,4)  | (3,1)  | (3,2)  |
|      |          | extended SOV 27 | 2.1311  | 2.3082 | 3.2734 | 3.8320 | 4.4962 | 4.7298 | 4.9138 |
|      |          | Present         | 2.1325  | 2.3075 | 3.2725 | 3.8325 | 4.4975 | 4.7275 | 4.9125 |
|      | 1.5      | Mode number     | (2,2)   | (1,3)  | (2,3)  | (3,1)  | (3,2)  | (1,4)  | (3,3)  |
|      |          | extended SOV 27 | 2.6277  | 3.4625 | 4.2915 | 4.7296 | 5.1259 | 5.7485 | 6.1588 |
|      |          | Present         | 2.6275  | 3.4625 | 4.2925 | 4.7275 | 5.1275 | 5.7475 | 6.1575 |



340 cients are defined as:

$$r_\xi = \frac{2ak_\xi^r}{D_{11}}, \quad (64a)$$

$$r_\eta = \frac{2bk_\eta^r}{D_{22}}. \quad (64b)$$

341 The first example considers a square isotropic plate with all four edges ro-  
 342 tationally restrained. The vertical translational springs along the four edges  
 343 are numerically set as  $k_{\xi=-1}^v = k_{\xi=1}^v = k_{\eta=-1}^v = k_{\eta=1}^v = 1 \times 10^{12} \text{ N m}^{-1}$ . The  
 344 material properties are given as  $D_{11} = D_{22} = D_3$  and  $\nu_{12} = \nu_{21} = 0.3$ .

345 Table 4 presents the frequency parameter  $2a\Omega$  for different rotational  
 346 stiffness coefficients  $r_\xi = r_\eta$  with values 0.1, 1, 10, 100, and 1000. Notably,  
 347 when  $r_\xi = r_\eta = 0$  and  $r_\xi = r_\eta = \infty$ , the boundary conditions correspond to  
 348 SSSS and CCCC, respectively.

349 Interestingly, the results indicate that the frequencies  $\Omega_x$  and  $\Omega_y$  are not  
 350 strictly equal for some mode shapes under rotationally restrained boundary  
 351 conditions. The actual frequency  $\Omega$  lies between  $\Omega_x$  and  $\Omega_y$ , which may be  
 352 attributed to the fact that  $\Omega_x$  and  $\Omega_y$  satisfy Rayleigh's principle in Equa-  
 353 tion (3), representing the weak-form governing equations, but do not nec-  
 354 essarily satisfy the strong-form governing equations in Equation (1). For a  
 355 physical problem with exact solutions, both Equations (1) and (3) must be  
 356 satisfied. If this condition is not met, applying Equation (3) still provides a  
 357 viable approach for approximating the exact solution of the plate. Thus, the  
 358 exact frequency can be estimated as  $\Omega = (\Omega_x + \Omega_y)/2$ . As shown in Table 4,  
 359 the maximum difference between  $\Omega$  and the solutions reported in 31 is less  
 360 than 1.3%. Figure 3 illustrates the variation in mode shapes corresponding  
 361 to the fundamental natural frequency as the rotational stiffness  $r_\xi = r_\eta$  in-  
 362 creases from zero to  $\infty$ , transitioning the boundary conditions from SSSS to  
 363 CCCC.

364 The next example considers a rectangular orthotropic plate with three  
 365 simply supported edges ( $k_{\xi=-1}^r = k_{\xi=1}^r = k_{\eta=1}^r = 0$ ), while the edge at  $\eta = -1$   
 366 is rotationally restrained. The material properties are consistent with those  
 367 in 31, where  $2D_{11} = 2D_{22} = D_3$  and  $\nu_{12} = \nu_{21} = 0.3$ . Table 5 shows the  
 368 fundamental frequency results for different length ratios ( $b/a$ ), comparing  
 369 them with those reported in 31. The maximum observed difference is 0.8%  
 370 when  $r_{\eta=-1} = 10$ .

371 In certain numerical calculations involving rotationally restrained bound-  
 372 ary conditions, the variables  $\alpha_1$  and  $\alpha_2$  may take complex values rather than

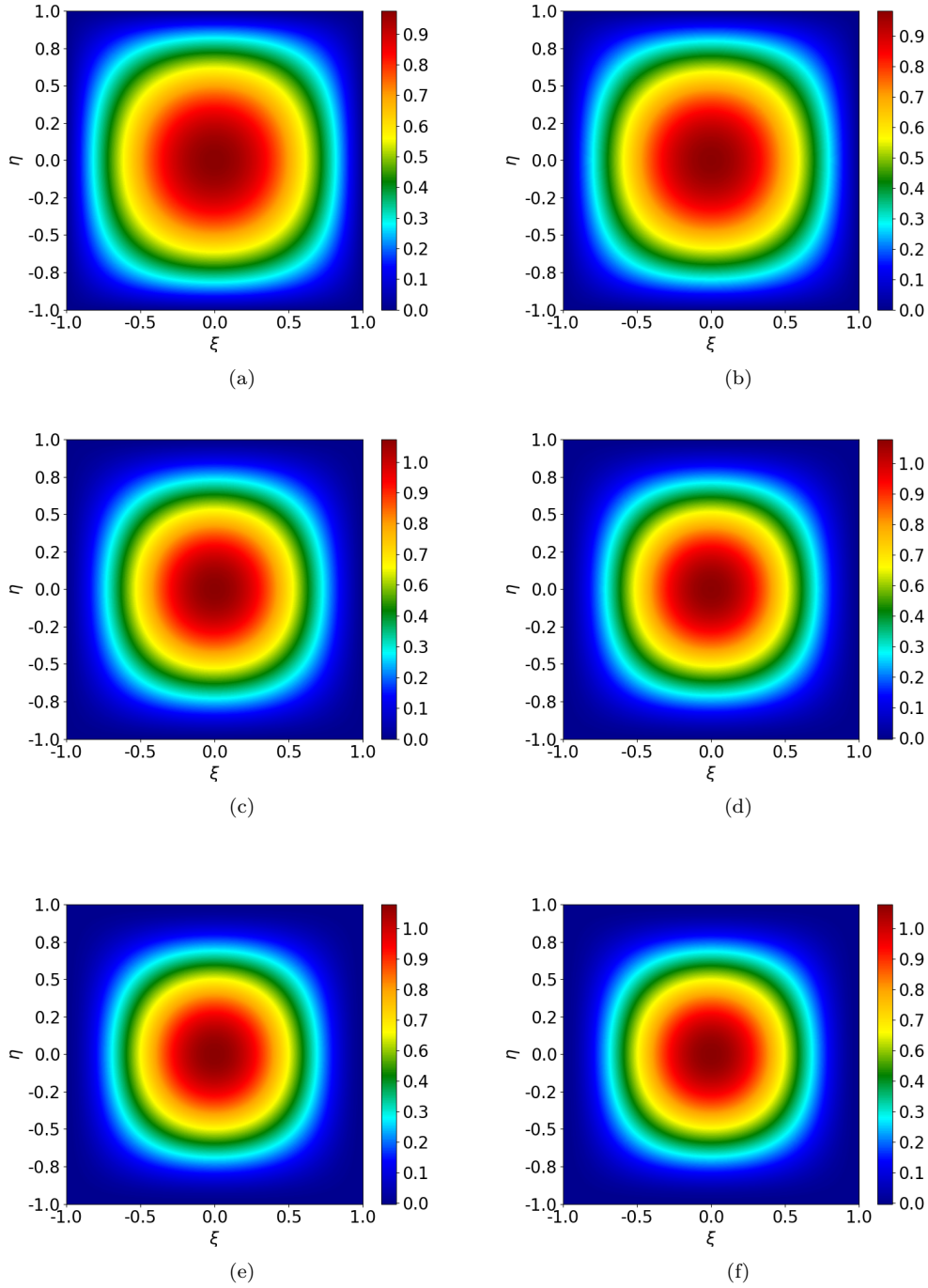


Figure 3: The first mode shape of a square isotropic plate with all four edges rotationally restrained: (a)  $r_\xi = r_\eta = 0$ ; (b)  $r_\xi = r_\eta = 1$ ; (c)  $r_\xi = r_\eta = 10$ ; (d)  $r_\xi = r_\eta = 20$ ; (e)  $r_\xi = r_\eta = 100$ ; (f)  $r_\xi = r_\eta = \infty$ .

Table 4: The first six frequency parameters,  $2a\Omega = 2a\sqrt[4]{\rho h\omega^2/D_{11}}$ , of a square isotropic plate with all four edges rotationally restrained, where  $k_{\xi=-1}^r = k_{\xi=1}^r = k_{\eta=-1}^r = k_{\eta=1}^r$ .

| $r$  | Mode                   | $2a\Omega$ |       |       |        |        |        |
|------|------------------------|------------|-------|-------|--------|--------|--------|
|      |                        | 1          | 2     | 3     | 4      | 5      | 6      |
| 0.1  | Mode number            | (1,1)      | (1,2) | (2,1) | (2,2)  | (1,3)  | (3,1)  |
|      | Ref.20                 | 4.454      | 6.992 | 7.045 | 8.890  | 9.782  | 9.960  |
|      | Ref.31                 | 4.465      | 7.039 | 7.039 | 8.897  | 9.945  | 9.945  |
|      | Present ( $\Omega_x$ ) | 4.463      | 7.028 | 7.043 | 8.893  | 9.938  | 9.953  |
|      | Present ( $\Omega_y$ ) | 4.463      | 7.043 | 7.028 | 8.893  | 9.953  | 9.938  |
|      | Present ( $\Omega$ )   | 4.463      | 7.035 | 7.035 | 8.893  | 9.945  | 9.945  |
|      | Difference (%)         | 0.044      | 0.056 | 0.056 | 0.044  | 0.000  | 0.000  |
| 1    | Mode number            | (1,1)      | (1,2) | (2,1) | (2,2)  | (3,1)  | (1,3)  |
|      | Ref.20                 | 4.529      | 7.008 | 7.136 | 8.936  | 9.787  | 10.036 |
|      | Ref.31                 | 4.637      | 7.155 | 7.155 | 8.991  | 10.029 | 10.030 |
|      | Present ( $\Omega_x$ ) | 4.648      | 7.098 | 7.223 | 8.993  | 10.093 | 9.968  |
|      | Present ( $\Omega_y$ ) | 4.648      | 7.223 | 7.098 | 8.993  | 9.968  | 10.098 |
|      | Present ( $\Omega$ )   | 4.648      | 7.160 | 7.160 | 8.993  | 10.030 | 10.033 |
|      | Difference (%)         | 0.237      | 0.069 | 0.069 | 0.022  | 0.009  | 0.029  |
| 10   | Mode number            | (1,1)      | (1,2) | (2,1) | (2,2)  | (1,3)  | (3,1)  |
|      | Ref.31                 | 5.346      | 7.768 | 7.768 | 9.537  | 10.552 | 10.563 |
|      | Present ( $\Omega_x$ ) | 5.413      | 7.718 | 7.953 | 9.598  | 10.448 | 10.782 |
|      | Present ( $\Omega_y$ ) | 5.413      | 7.953 | 7.718 | 9.598  | 10.782 | 10.453 |
|      | Present ( $\Omega$ )   | 5.413      | 7.835 | 7.835 | 9.598  | 10.615 | 10.618 |
|      | Difference (%)         | 1.253      | 0.862 | 0.862 | 0.639  | 0.597  | 0.520  |
| 100  | Mode number            | (1,1)      | (1,2) | (2,1) | (2,2)  | (1,3)  | (3,1)  |
|      | Ref.20                 | 5.895      | 8.326 | 8.422 | 10.167 | 10.957 | 11.297 |
|      | Ref.31                 | 5.901      | 8.442 | 8.442 | 10.253 | 11.307 | 11.333 |
|      | Present ( $\Omega_x$ ) | 5.913      | 8.428 | 8.473 | 10.258 | 11.293 | 11.373 |
|      | Present ( $\Omega_y$ ) | 5.913      | 8.473 | 8.478 | 10.258 | 11.373 | 11.293 |
|      | Present ( $\Omega$ )   | 5.913      | 8.450 | 8.450 | 10.258 | 11.333 | 11.333 |
|      | Difference (%)         | 0.203      | 0.094 | 0.094 | 0.048  | 0.229  | 0.000  |
| 1000 | Mode number            | (1,1)      | (1,2) | (2,1) | (2,2)  | (1,3)  | (3,1)  |
|      | Ref.31                 | 6.011      | 8.585 | 8.585 | 10.424 | 11.495 | 11.522 |
|      | Present ( $\Omega_x$ ) | 5.988      | 8.553 | 8.553 | 10.388 | 11.463 | 11.478 |
|      | Present ( $\Omega_y$ ) | 5.988      | 8.553 | 8.553 | 10.388 | 11.478 | 11.463 |
|      | Present ( $\Omega$ )   | 5.988      | 8.553 | 8.553 | 10.388 | 11.470 | 11.470 |
|      | Difference (%)         | 0.382      | 0.372 | 0.372 | 0.345  | 0.217  | 0.451  |

being purely real. Consequently, the mode shape coefficients  $A_1$ ,  $A_2$ ,  $B_1$ , and  $B_2$  become complex-valued, leading to  $\mathbf{R}$  and  $\mathbf{Q}^{-1}$  being complex matrices. However, the mode shapes  $\phi(\xi)$  and  $\psi(\eta)$  remain real-valued, and the dynamic stiffness matrix  $\mathbf{K} = \mathbf{R}\mathbf{Q}^{-1}$  is a real symmetric matrix. Thus, the frequency  $\Omega$  can be obtained by solving  $\mathbf{K}$  using the refined W-W algorithm provided in this study, which avoids solving the eigenvalue equations in both the real and complex domains.

Table 5: Fundamental frequency parameter  $2a\Omega = 2a\sqrt[4]{\rho h\omega^2/D_{11}}$  of rectangular orthotropic plates with three edges simply supported ( $k_{\xi=-1}^r = k_{\xi=1}^r = k_{\eta=1}^r = 0$ ) and the edge at  $\eta = -1$  rotationally restrained.

| $b/a$ | $r_{\eta=-1}$ | $2a\Omega$ |                      |                        |                        |                |
|-------|---------------|------------|----------------------|------------------------|------------------------|----------------|
|       |               | Ref.31     | Present ( $\Omega$ ) | Present ( $\Omega_x$ ) | Present ( $\Omega_y$ ) | Difference (%) |
| 0.5   | 0             | 7.530      | 7.523                | 7.523                  | 7.523                  | 0.092          |
|       | 1             | 7.690      | 7.700                | 7.588                  | 7.813                  | 0.130          |
|       | 10            | 8.250      | 8.308                | 8.198                  | 8.418                  | 0.703          |
|       | $\infty$      | 8.705      | 8.695                | 8.695                  | 8.695                  | 0.114          |
| 1.0   | 0             | 4.917      | 4.918                | 4.918                  | 4.918                  | 0.020          |
|       | 1             | 4.954      | 4.960                | 4.933                  | 4.988                  | 0.121          |
|       | 10            | 5.114      | 5.128                | 5.088                  | 5.168                  | 0.273          |
|       | $\infty$      | 5.289      | 5.278                | 5.278                  | 5.278                  | 0.207          |
| 1.5   | 0             | 4.126      | 4.128                | 4.128                  | 4.128                  | 0.048          |
|       | 1             | 4.139      | 4.138                | 4.128                  | 4.148                  | 0.024          |
|       | 10            | 4.202      | 4.208                | 4.188                  | 4.228                  | 0.142          |
|       | $\infty$      | 4.292      | 4.288                | 4.288                  | 4.288                  | 0.093          |

## 5. Conclusion

In this study, the dynamic stiffness matrix (DSM) based on the extended separation-of-variable (SOV) type solution has been developed for the vibration analysis of an orthotropic rectangular plate with general homogeneous boundary conditions.

Instead of solving highly nonlinear eigenvalue equations involved in the SOV methods, the extended SOV type solution is adopted to construct the

dynamic stiffness matrices. Several novel techniques have proposed to solve the eigenvalue problem and mode shape computation. The challenge of determining the fully clamped frequencies using the Wittrick-Williams (W-W) algorithm is resolved by computing the frequencies under specific boundary conditions, whose closed-form expression can be easily derived using the SOV method.

Classical boundary conditions, such as guided, simply supported, clamped, and free edges, can be realized by setting the translational springs ( $k_\xi^v$ ) and rotational springs ( $k_\xi^r$ ) along the plate edges to either zero or infinity. Numerical experiments have validated accuracy of this approach for these boundary conditions. The results shows that the SOV type solution can also be extended to handle elastically restrained boundary conditions. Despite certain approximations inherent in some elastically restrained cases, the maximum percentage error across all numerical experiments remains within 1.25%. This may occur because the SOV type solution used is derived from the weak-form governing equation, which is based on Rayleigh's principle.

Since the SOV type solution  $\phi(\xi)\psi(\eta)$  consists of only a single term for each mode order, unlike the infinite series expansions used in the traditional DSM, each eigenvalue solution can be explicitly expressed. This suggests the potential for obtaining more concise solutions for assembled plate structures compared to traditional DSM methods.

## Appendix A Integral parameters

The integral parameters  $I_1$ ,  $I_2$ ,  $I_3$ , and  $I_4$  are defined as follows:

$$\begin{aligned}
I_1 &= \int_0^1 \psi^2 d\eta \\
&= (B_1^2 + B_2^2 - B_3^2 + B_4^2) + \frac{-B_1^2 + B_2^2}{2\alpha_2} \sin(2\alpha_2) + \frac{B_3^2 + B_4^2}{2\beta_2} \sinh(2\beta_2) \\
&\quad + \frac{4(\alpha_2 B_2 B_4 + \beta_2 B_1 B_3)}{\alpha_2^2 + \beta_2^2} \sin(\alpha_2) \cosh(\beta_2) \\
&\quad + \frac{4(-\alpha_2 B_1 B_3 + \beta_2 B_2 B_4)}{\alpha_2^2 + \beta_2^2} \cos(\alpha_2) \sinh(\beta_2).
\end{aligned} \tag{A.1}$$

410

$$\begin{aligned}
I_2 &= \int_0^1 \left( \psi \frac{d^2 \psi}{d\eta^2} \right) d\eta \\
&= \left( -\alpha_2^2 B_1^2 - \alpha_2^2 B_2^2 - \beta_2^2 B_3^2 + \beta_2^2 B_4^2 \right) \\
&\quad + \frac{\alpha_2(B_1^2 - B_2^2)}{2} \sin(2\alpha_2) + \frac{\beta_2(B_3^2 + B_4^2)}{2} \sinh(2\beta_2) \\
&\quad + \frac{2(-\alpha_2^2 + \beta_2^2)(\alpha_2 B_2 B_4 + \beta_2 B_1 B_3)}{\alpha_2^2 + \beta_2^2} \sin(\alpha_2) \cosh(\beta_2) \\
&\quad + \frac{2(-\alpha_2^2 + \beta_2^2)(-\alpha_2 B_1 B_3 + \beta_2 B_2 B_4)}{\alpha_2^2 + \beta_2^2} \cos(\alpha_2) \sinh(\beta_2).
\end{aligned} \tag{A.2}$$

411

$$\begin{aligned}
I_3 &= \int_0^1 \left( \frac{d\psi}{d\eta} \right)^2 d\eta \\
&= \alpha_2^2 B_1^2 + \alpha_2^2 B_2^2 + \beta_2^2 B_3^2 - \beta_2^2 B_4^2 \\
&\quad + \frac{\alpha_2(B_1^2 - B_2^2)}{2} \sin(2\alpha_2) + \frac{\beta_2(B_3^2 + B_4^2)}{2} \sinh(2\beta_2) \\
&\quad + \frac{4\alpha_2\beta_2(\alpha_2 B_1 B_3 - \beta_2 B_2 B_4)}{\alpha_2^2 + \beta_2^2} \sin(\alpha_2) \cosh(\beta_2) \\
&\quad + \frac{4\alpha_2\beta_2(\alpha_2 B_2 B_4 + \beta_2 B_1 B_3)}{\alpha_2^2 + \beta_2^2} \cos(\alpha_2) \sinh(\beta_2).
\end{aligned} \tag{A.3}$$

412

$$\begin{aligned}
I_4 &= \int_0^1 \left( \frac{d^2 \psi}{d\eta^2} \right)^2 d\eta \\
&= \left( \alpha_2^4 B_1^2 + \alpha_2^4 B_2^2 - \beta_2^4 B_3^2 + \beta_2^4 B_4^2 \right) \\
&\quad + \frac{\alpha_2^3(-B_1^2 + B_2^2)}{2} \sin(2\alpha_2) + \frac{\beta_2^3(B_3^2 + B_4^2)}{2} \sinh(2\beta_2) \\
&\quad + \frac{4\alpha_2^2\beta_2^2(-\alpha_2 B_2 B_4 - \beta_2 B_1 B_3)}{\alpha_2^2 + \beta_2^2} \sin(\alpha_2) \cosh(\beta_2) \\
&\quad + \frac{4\alpha_2^2\beta_2^2(\alpha_2 B_1 B_3 - \beta_2 B_2 B_4)}{\alpha_2^2 + \beta_2^2} \cos(\alpha_2) \sinh(\beta_2)
\end{aligned} \tag{A.4}$$

413 The integral parameters  $J_1$ ,  $J_2$ ,  $J_3$ , and  $J_4$  can be obtained by replacing  $B_1$   
414 to  $B_4$  by  $A_1$  to  $A_4$ , respectively, and  $\alpha_2$  and  $\beta_2$  by  $\alpha_1$  and  $\beta_1$ , respectively.

## 415 References

- 416 [1] Banerjee, J., Papkov, S., Liu, X., Kennedy, D., 2015. Dynamic stiffness  
417 matrix of a rectangular plate for the general case. *Journal of Sound and*  
418 *Vibration* 342, 177–199. doi:10.1016/j.jsv.2014.12.031.
- 419 [2] Banerjee, J.R., 1997. Dynamic stiffness formulation for structural el-  
420 ements: a general approach. *Computers & Structures* 63, 101–103.  
421 doi:10.1016/S0045-7949(96)00326-4.
- 422 [3] Biancolini, M.E., Brutti, C., Reccia, L., 2005. Approximate solution for  
423 free vibrations of thin orthotropic rectangular plates. *Journal of Sound*  
424 *and Vibration* 288, 321–344. doi:10.1016/j.jsv.2005.01.005.
- 425 [4] Boscolo, M., Banerjee, J., 2011. Dynamic stiffness elements and their ap-  
426 plications for plates using first order shear deformation theory. *Comput-*  
427 *ers & Structures* 89, 395–410. doi:10.1016/j.compstruc.2010.11.005.
- 428 [5] Fazzolari, F., Boscolo, M., Banerjee, J., 2013. An exact dynamic stiffness  
429 element using a higher order shear deformation theory for free vibration  
430 analysis of composite plate assemblies. *Composite Structures* 96, 262–  
431 278. doi:10.1016/j.compstruct.2012.08.033.
- 432 [6] Ghorbel, O., Casimir, J.B., Hammami, L., Tawfiq, I., Haddar, M., 2015.  
433 Dynamic stiffness formulation for free orthotropic plates. *Journal of*  
434 *Sound and Vibration* 346, 361–375. doi:10.1016/j.jsv.2015.02.020.
- 435 [7] Gorman, D.J., 2005. Free in-plane vibration analysis of rectangular  
436 plates with elastic support normal to the boundaries. *Journal of Sound*  
437 *and Vibration* 285, 941–966. doi:10.1016/j.jsv.2004.09.017.
- 438 [8] Han, F., Dan, D., Cheng, W., Zang, J., 2018. An improved wittrick-  
439 williams algorithm for beam-type structures. *Composite Structures* 204,  
440 560–566. doi:10.1016/j.compstruct.2018.07.108.
- 441 [9] Kantorovich, L.V., Krylov, V.I., 1958. Approximate Methods of Higher  
442 Analysis. Interscience Publishers, New York.
- 443 [10] Kerr, A.D., 1968. An extension of the kantorovich method. *Quarterly*  
444 *of Applied Mathematics* 26, 219–229. doi:10.1090/qam/99857.

- 445 [11] Khov, H., Li, W.L., Gibson, R.F., 2009. An accurate solution method  
446 for the static and dynamic deflections of orthotropic plates with general  
447 boundary conditions. *Composite Structures* 90, 474–481. doi:10.1016/  
448 j.compstruct.2009.04.020.
- 449 [12] Laura, P.A., Saffell Jr, B.F., 1967. Study of small-amplitude vibrations  
450 of clamped rectangular plates using polynomial approximations. *The*  
451 *Journal of the Acoustical Society of America* 41, 836–839. doi:10.1121/  
452 1.1910414.
- 453 [13] Leissa, A.W., 1973. The free vibration of rectangular plates. *Jour-*  
454 *nal of Sound and Vibration* 31, 257–293. doi:10.1016/S0022-460X(73)  
455 80371-2.
- 456 [14] Levy, M., 1899. Sur l’équilibre élastique d’une plaque rectangulaire.  
457 *Comptes Rendus Acad. Sci. Paris* 129, 535–539.
- 458 [15] Li, R., Zhong, Y., Tian, B., Liu, Y., 2009a. On the finite integral trans-  
459 form method for exact bending solutions of fully clamped orthotropic  
460 rectangular thin plates. *Applied Mathematics Letters* 22, 1821–1827.  
461 doi:10.1016/j.aml.2009.07.003.
- 462 [16] Li, W.L., 2004. Vibration analysis of rectangular plates with general  
463 elastic boundary supports. *Journal of Sound and Vibration* 273, 619–  
464 635. doi:10.1016/S0022-460X(03)00562-5.
- 465 [17] Li, W.L., Zhang, X., Du, J., Liu, Z., 2009b. An exact series solu-  
466 tion for the transverse vibration of rectangular plates with general elas-  
467 tic boundary supports. *Journal of Sound and Vibration* 321, 254–269.  
468 doi:10.1016/j.jsv.2008.09.035.
- 469 [18] Liu, X., Banerjee, J., 2015. An exact spectral-dynamic stiffness  
470 method for free flexural vibration analysis of orthotropic composite  
471 plate assemblies—part i: Theory. *Composite Structures* 132, 1274–1287.  
472 doi:10.1016/j.compstruct.2015.07.020.
- 473 [19] Liu, X., Banerjee, J., 2016. Free vibration analysis for plates with  
474 arbitrary boundary conditions using a novel spectral-dynamic stiff-  
475 ness method. *Computers & Structures* 164, 108–126. doi:10.1016/  
476 j.compstruc.2015.11.005.



- 477 [20] Mukhopadhyay, M., 1979. Free vibration of rectangular plates with  
478 edges having different degrees of rotational restraint. *Journal of Sound*  
479 *and Vibration* 67, 459–468.
- 480 [21] Navier, L., 1823. Extrait des recherches sur la flexion des plans elas-  
481 tiques. *Bull. Sci. Soc. Philomat.* , 95–102.
- 482 [22] Timoshenko, S., 1940. *Theory of Plates and Shells*. McGraw-Hill Book  
483 Company.
- 484 [23] Wittrick, W.H., Williams, F.W., 1971. A general algorithm for comput-  
485 ing natural frequencies of elastic structures. *The Quarterly Journal of*  
486 *Mechanics and Applied Mathematics* 24, 263–284. doi:10.1093/qjmam/  
487 24.3.263.
- 488 [24] Xing, Y., Li, G., Yuan, Y., 2022. A review of the analytical solution  
489 methods for the eigenvalue problems of rectangular plates. *International*  
490 *Journal of Mechanical Sciences* 221, 107171. doi:10.1016/j.ijmecsci.  
491 2022.107171.
- 492 [25] Xing, Y., Liu, B., 2009a. New exact solutions for free vibrations of  
493 rectangular thin plates by symplectic dual method. *Acta Mechanica*  
494 *Sinica* 25, 265–270. doi:10.1007/s10409-008-0208-4.
- 495 [26] Xing, Y., Sun, Q., Liu, B., Wang, Z., 2018. The overall assessment  
496 of closed-form solution methods for free vibrations of rectangular thin  
497 plates. *International Journal of Mechanical Sciences* 140, 455–470.  
498 doi:10.1016/j.ijmecsci.2018.03.013.
- 499 [27] Xing, Y., Wang, Z., 2020a. An extended separation-of-variable method  
500 for the free vibration of orthotropic rectangular thin plates. *International*  
501 *Journal of Mechanical Sciences* 182, 105739. doi:10.1016/j.ijmecsci.  
502 2020.105739.
- 503 [28] Xing, Y., Wang, Z., 2020b. An improved separation-of-variable method  
504 for the free vibration of orthotropic rectangular thin plates. *Composite*  
505 *Structures* 252, 112664. doi:10.1016/j.compstruct.2020.112664.
- 506 [29] Xing, Y.F., Liu, B., 2009b. New exact solutions for free vibrations of  
507 thin orthotropic rectangular plates. *Composite Structures* 89, 567–574.  
508 doi:10.1016/j.compstruct.2008.11.010.

- 509 [30] Yuan, S., Ye, K., Williams, F., 2004. Second order mode-finding method  
510 in dynamic stiffness matrix methods. *Journal of Sound and Vibration*  
511 269, 689–708. doi:10.1016/S0022-460X(03)00126-3.
- 512 [31] Zhang, S., Xu, L., Li, R., 2019. New exact series solutions for transverse  
513 vibration of rotationally-restrained orthotropic plates. *Applied Mathe-*  
514 *matical Modelling* 65, 348–360. doi:10.1016/j.apm.2018.08.033.
- 515 [32] Zhong, W.X., 1995. A new systematic methodology for theory of elas-  
516 ticity. Dalian University of Technology Press, Dalian , 182–187.
- 517 [33] Zhong, Y., Zhao, X.F., Li, R., 2013. Free vibration analysis of rectangu-  
518 lar cantilever plates by finite integral transform method. *International*  
519 *Journal for Computational Methods in Engineering Science and Me-*  
520 *chanics* 14, 221–226. doi:10.1080/15502287.2012.711424.